

https://dspace.org/

Extremely rapid yet noncatastrophic preservation of the flattenedfeathered and 3D dinosaurs of the Early Cretaceous of China

Scott MacLennan; J Sha; P.E Olsen; S.T Kinney; Et al

https://hdl.handle.net/10539/43469
WOS

Downloaded from a DSpace repository. https://dspace.org/

PNAS RESEARCH ARTICLE | EARTH, ATMOSPHERIC, AND PLANETARY SCIENCES
EVOLUTION

Extremely rapid, yet noncatastrophic, preservation of the flattened-feathered and 3D dinosaurs of the Early Cretaceous of China

Scott A. MacLennan[a,b,1], Jingeng Sha[c,1], Paul E. Olsen[d,1], Sean T. Kinney[d], Clara Chang[d], Yanan Fang[c], Jun Liu[e], Bennett B. Slibeck[d], Elaine Chen[f], and Blair Schoene[b]

Affiliations are included on p. 6.

Contributed by Paul E. Olsen; received February 20, 2024; accepted August 27, 2024; reviewed by Terrence Blackburn, Bhart-Anjan S. Bhullar, and E. T. Rasbury

Northeast China's Early Cretaceous Yixian Formation preserves spectacular fossils that have proved extraordinarily important in testing evolutionary hypotheses involving the origin of birds and the distribution of feathers among nonavian dinosaurs. These fossils occur either flattened with soft tissue preservation (including feathers and color) in laminated lacustrine strata or as three-dimensional (3D) skeletons in "life-like" postures in more massive deposits. The relationships of these deposits to each other, their absolute ages, and the origin of the extraordinary fossil preservation have been vigorously debated for nearly a half century, with the prevailing view being that preservation was linked to violent volcanic eruptions or lahars, similar to processes that preserved human remains at Pompeii. We present high-precision zircon U-Pb geochronology from cores and outcrops, demonstrating that Yixian Formation accumulation rates are more than an order of magnitude higher than usually estimated. Additionally, we provide zircon provenance and sedimentological data from 3D dinosaur fossils, which imply that their death and burial occurred in collapsed burrows, rather than via a catastrophic volcanogenic mechanism. In the studied area, the three principal fossil-rich intervals of the Yixian occur as a cyclic sequence that correspond to periods of high precipitation. Using Bayesian–Markov Chain Monte Carlo approaches, we constrain the total duration of the sequence to less than ~93,000 y and suggest that climatic precession paced the expression of these cyclic sediments. Rather than representing multiple, Pompeii-like catastrophes, the Yixian Formation is instead a brief snapshot of normal life and death in an Early Cretaceous continental community.

Jehol Biota | Early Cretaceous | U-Pb geochronology | lacustrine astrochronology | taphonomy

Significance

Traditionally, the spectacular preservation of fossils of feathered dinosaurs and early birds and other animals found in sedimentary strata of the Yixian Formation in northeast China has been attributed to Pompeii-like volcanic catastrophes. We provide high-resolution geochronology and sedimentological analysis challenging this model and show that these strata instead record normal life and death processes preserved in a succession of depositional environments that span less than 100 thousand years.

The continental, Early Cretaceous age Yixian Formation in Liaoning and Inner Mongolia, China, preserves remarkable fossil assemblages, broadly termed the Jehol Biota, that have revolutionized our understanding of dinosaurian paleobiology and Early Cretaceous ecosystems (1–6). In the areas near the villages of Sihetun, Huangbanjigou, and Lujiatun, these fossil assemblages occur in two famously productive, distinct lithostratigraphic members. Flattened feathered dinosaurs and other organisms with soft tissues are preserved in the lacustrine Jianshangou Member (7, 8), and three-dimensional (3D), perfectly articulated skeletons in life-like postures and associated with apparent nests are found in the Lujiatun Member (8, 9). The mechanism for the seemingly exceptional preservation of these organisms remains contested (e.g., refs. 10 and 11), however, the most commonly favored model (6, 11–14), requires the influence of catastrophic burial in pyroclastics akin to the Vesuvian eruption at Pompeii in AD 79. Indeed, these fossil sites have nicknames that are versions of "China's Cretaceous" Pompeii (6, 11–15). In addition, the temporal and environmental relationships for these assemblages with their divergent taphonomic motifs also remain contentious, impeding a synoptic view of this critical window into Early Cretaceous life.

Major paleobiologically and paleoclimatologically relevant issues regarding the stratigraphic units containing the Jehol biota include: 1) whether the Jianshangou Member with lacustrine flattened fossil assemblages is temporally equivalent to the more terrestrial Lujiatun Member with fossil skeletons preserved in 3D (16, 17), or if these members represent different styles of preservation in successive environments; 2) what time duration the Lujiatun and Jianshangou members record and whether the sedimentological evidence for apparently cyclic environmental fluctuations are orbitally paced at precession (10s of kyr) or eccentricity (100s of kyr) frequencies (11, 18); and 3) whether the Yixian fauna represents catastrophic death assemblages with animals entombed in pyroclastic flows, ashes, or lahars as interpreted by previous studies (6, 11–14) or if more mundane attritional

Author contributions: S.A.M., J.S., S.T.K., P.E.O., and Y.F. designed research; S.A.M., S.T.K., P.E.O., C.C., J.L., B.B.S., E.C., and B.S. performed research; S.A.M., S.T.K., P.E.O., C.C., and B.S. analyzed data; S.A.M. conceptualized project; J.S. and S.T.K. funding; P.E.O. conceptualized project, drafted figures, project administration and supervision, funding; and S.A.M., S.T.K., and P.E.O. wrote the paper.

Reviewers: T.B., University of California, Santa Cruz; B.-A.S.B., Yale University; and E.T.R., Stony Brook University.

The authors declare no competing interest.

Copyright © 2024 the Author(s). Published by PNAS. This article is distributed under Creative Commons Attribution-NonCommercial-NoDerivatives License 4.0 (CC BY-NC-ND).

[1]To whom correspondence may be addressed. Email: scott.maclennan@wits.ac.za, jgsha@nigpas.ac.cn, or polsen@ldeo.columbia.edu.

This article contains supporting information online at https://www.pnas.org/lookup/suppl/doi:10.1073/pnas.2322875121/-/DCSupplemental.

Published November 4, 2024.

Downloaded from https://www.pnas.org by Paul Olsen on November 4, 2024 from IP address 67.85.115.75.

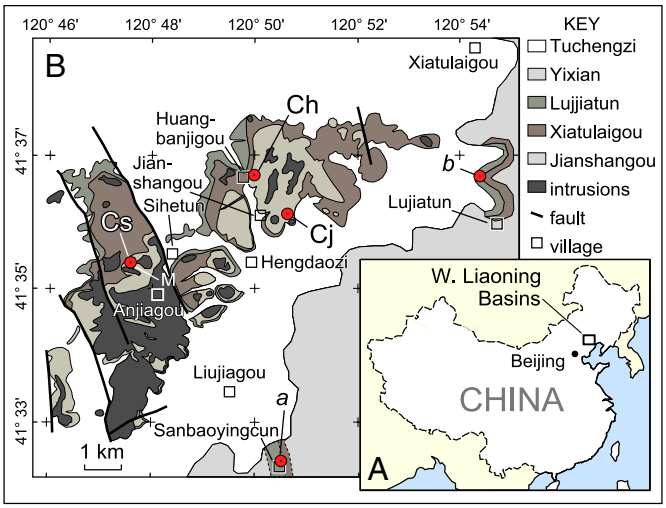


Fig. 1. Location of cores and outcrops. (*A*) Index map showing the location of study area in Liaoning Province, China. (*B*) Geologic map showing key localities (*SI Appendix*, Table S1): *a*, location of Sanbaoyingcun sample; *b*, type section of the Lujiatun Member (8); Ch, Core 1 (Huangbanjiagou no. 1); Cj, Jainshangou no. 1 core; Cs, Core 2 (Sihetun no. 1). Figure adapted from ref. 8 with permission from Elsevier, in which complete core descriptions are found.

models can be applied. Recently published high-resolution $^{40}Ar/^{39}Ar$ and U-Pb geochronological studies have not provided resolution to these problems (16, 19).

To address these issues, we use stratigraphic and sedimentological analysis of drill core and outcrops, U-Pb zircon geochronology via thermal ionization mass spectrometry (TIMS) and a Bayesian statistical approach (20) and laser ablation inductive coupled mass spectrometry (LA-ICP-MS), Huangbanjiagou (8) and Sihetun (Figs. 1 and 2 and *SI Appendix*, Figs. S1–S4), which, critically, contain what we argue are complete sequences of the lower Yixian Formation in unambiguous stratigraphic superposition. Our samples come from within the fossiliferous Lujiatun and Jianshangou Members, including an outcrop exposure of the Lujiatun Member from an area that produced many articulated dinosaurs, as well as matrix from two blocks containing 3D-preserved articulated dinosaurs from this locality. Our integrated geological context allows for the construction of a high-precision age model for the local stratigraphy, permitting tests of hypotheses concerning the contemporaneity of stratigraphic members, orbital pacing of cyclic sediments, and mode of preservation (Figs. 2 and 3).

The prevalent interpretation of lower Yixian Formation stratigraphy (hypothesis 1 in Fig. 2*A*) has the Jianshangou Member deep-water lake sequence laterally equivalent to the outcropping, 3D-dinosaur-producing, supposedly shoreline facies Lujiatun Member outcrops. This hypothesis requires two lava flow sequences, two Lujiatun-like units, and requires that the Xiatulaigou Member flows (Lava 1 in Fig. 2) were not deposited in the Lujiatun area. Here, we present a more parsimonious hypothesis (hypothesis 2 in Fig. 2*A*) that correlates the Lujiatun outcrop with the Lujiatun-like unit in the drillcore and requires only one lava flow sequence (Xiatulaigou Member) and one Lujiatun-like unit. In hypothesis 2, the Jianshangou member is missing due to erosion in the Lujiatun outcrop area.

Critical to testing these hypotheses is drill core Huangbanjigou No. 1 (Ch in Fig. 1, hereafter termed Core 1), which was drilled directly adjacent to quarries producing typical faunal assemblages of the Jianshangou Member. It spans the complete local stratigraphy of lacustrine finely laminated siliciclastics of the Jianshangou Member with numerous crystal-rich airfall tuffs, the underlying basaltic lavas of the Xiatulaigou Member, and a lower unit characterized by mixed fine and coarse siliciclastics and volcaniclastics that we interpret as representing the Lujiatun Member. These rocks unconformably overlie the Tuchengzi Formation (8) (Figs. 1 and 2 and *SI Appendix*, Fig. S2). The Yixian stratigraphy in this core is very similar to that intersected by another core recovered at the Sihuten geopark, (Sihetun no. 1, Cs in Fig. 1, hereafter Core 2). The basal part of the stratigraphy intersected by core 1 is also similar to outcrops from the Lujiatun Member to the east, where exquisite tetrapod skeletons have been recovered (Fig. 2), but where the overlying Jianshangou Member is not preserved.

Two horizons within core 1 were sampled for U-Pb geochronology. Sample H1-8810 is located at the base of core 1, within siliciclastics in what we hypothesize to be the Lujiatun Member (Fig. 2). This sample is a fluvially reworked volcanoclastic unit based on the presence of stratigraphically proximal polymict conglomerates, and lithic clasts in the sample itself (*SI Appendix*, Fig. S9). A graded airfall tuff (sample H1-3794) associated with the microlaminated lower Jianshangou Member, which overlies the Xiatulaigou Member lavas, was sampled near the middle of the drill core (*SI Appendix*, Figs. S4 and S8). This portion of the drill core bears *Eoestheria* (a clam shrimp) and *Lycoptera* (a teleost fish), typical elements of the Jehol Biota (25). A thin airfall tuff near the local top of the Jianshangou Member (sample 09.22.15-01) was sampled from outcrop adjacent to the drill core and is our highest sample in the local stratigraphy (Fig. 2 and *SI Appendix*, Figs. S3 and S7).

In addition to drill-core-focused-sampling, matrix of two museum specimens of perfectly articulated 3D *Psittacosaurus* (Ceratopsia, Ornithischia) specimens [Institute of Vertebrate Paleontology and Paleoanthropology (Beijing) (IVPP) 18343 and 18344] from the Lujiatun Member outcrops at Sanbaoyingcun, typical of the preservation style of the member, were sampled to determine grain size and detrital zircon provenance (Fig. 3 and *SI Appendix*, Figs. S1, S5, S6, S11, and S12). Samples were collected from both adjacent to the femur and at the edge of the blocks, as far from the skeleton for each specimen as possible. We also collected volcanoclastic mudstone from an outcrop in the same area (sample 09.18.15-05) for geochronological and provenance purposes. The resulting Bayesian–MCMC high-precision age model for the local stratigraphy and provenance and petrological observations on the fossil-bearing volcano-sedimentary rocks permit the testing of the hypotheses outlined above.

Results

We acquired high-precision TIMS U-Pb ages for the three samples from, and adjacent to, core 1 (Fig. 2*B*), as well as for the sample from outcrop at Sanbaoyingcun (*SI Appendix*, section 2b, Fig. S18, and Table S2). The depositional ages of these zircon-bearing volcaniclastic horizons were estimated using a Bayesian-MCMC method (20). These depositional ages were then used to establish a Bayesian, stratigraphic age model for core 1 (Fig. 1). The depositional age estimates for the four samples that span the stratigraphy at Huangbanjigou, and the Bayesian stratigraphic age model derived from them, show that Yixian Formation sediments in the Sihetun-Huangbanjigou area record an extremely short time period of 49 +40/–49 kyrs at this locality (Fig. 2). A distribution of duration estimates for lower Yixian Formation deposition arise from our age model and the 99th percentile of this distribution is ~93 kyr, implying that it is extremely unlikely that deposition of the Yixian Formation in this area lasted for more than 100 kyr. While there are indications of fluvial reworking of the Lujiatun Member in core, outcrop and thin section (*SI Appendix*, Figs. S9–S13), the graded tuff bed in the middle of the Jianshangou

Downloaded from https://www.pnas.org by Paul Olsen on November 4, 2024 from IP address 67.85.115.75.

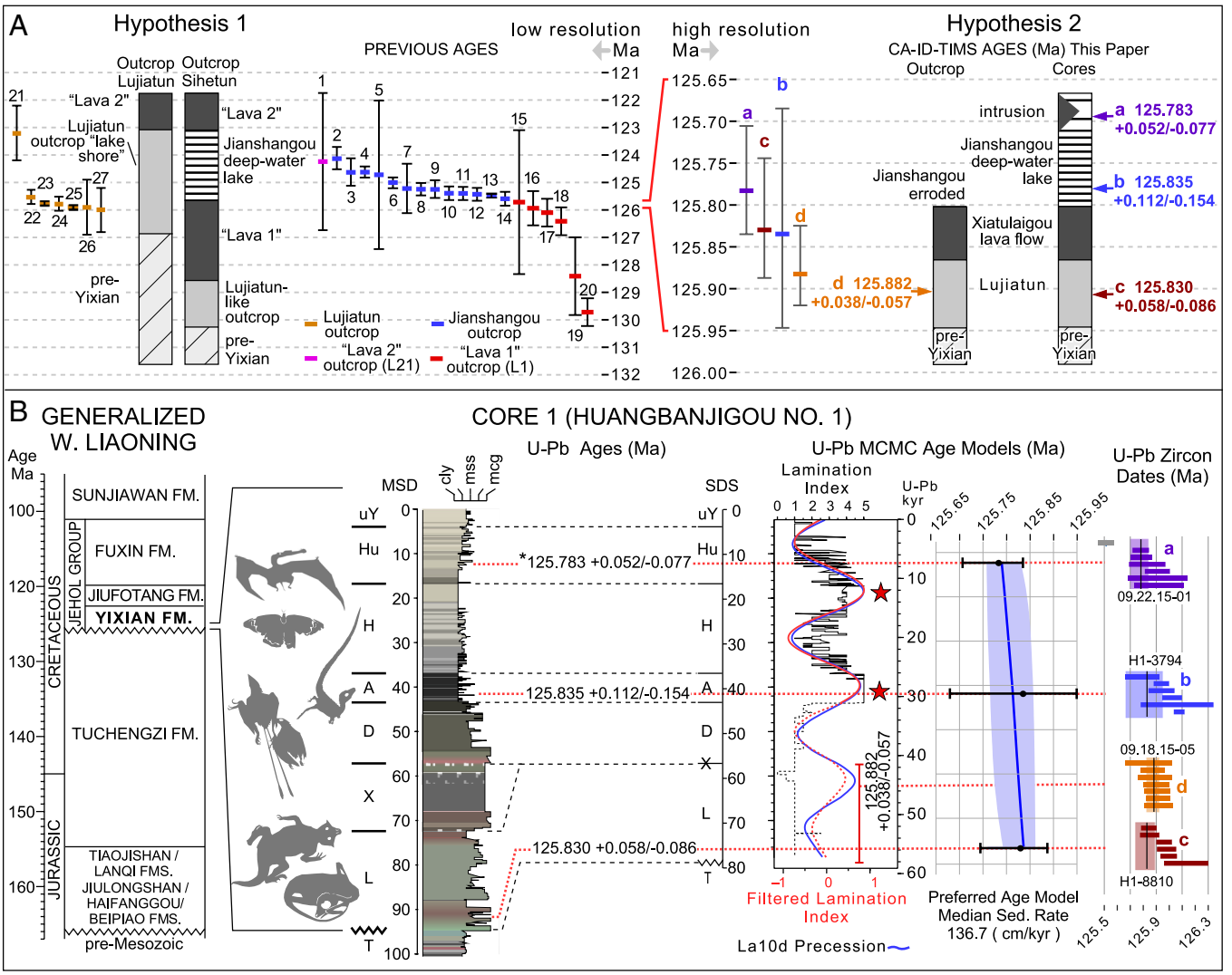


Fig. 2. Temporal constraints and hypotheses for relationships between fossil-bearing units of the Yixian Formation. (*A*) Diagrammatic representation of the two hypotheses for correlation of the Yixian Formation in the Sihetun-Huangbanjiagou area (cores) to Lujiatun area (outcrop) with geochronological constraints. The vertical axis (time) of each hypothesis is shown separately with the axis for Hypothesis 2 (*Right*) being a greatly expanded, high-resolution portion of that for Hypothesis 1 (*Left*). Note that the low-resolution (and inaccurate) previous ages allowed for the "Lava 1" to be largely older than the Lujiatun outcrop, while the core stratigraphy and ages do not. Key to ages 1 to 27 in *SI Appendix*, Table S4. (*B*) CA-ID-TIMS zircon ages (this paper), Bayesian Markov Chain Monte Carlo (MCMC) eruption ages (black circles with black error bars) and stratigraphic age model (dark blue model mean with blue shaded area indicating 95% credible interval) and lithologic section of the Yixian Formation in Core 1 (Huangbanjigou no. 1). Sample designated by * is from outcrop adjacent to core 1 and sample 09.18.15-05 is from a more distant outcrop of the Lujiatun Member at Sanbaoyingcun (Fig. 1). Red stars indicate the stratigraphic positions of the major fossil producing Anjiagou and Hengdaozi beds. Fauna silhouettes based on refs. 3, and 21–24, see *SI Appendix*, pt. 1 for outcrop and core details and are placed to the immediate left of the approximate stratigraphic level that produced them. Lithostratigraphic units: uY, undivided Yixian Formation; Hu, Huangbanjigou Bed, Jianshangou Member; H, Hengdaozi Bed, Jianshangou Member; A, Anjiagou Bed, Jianshangou Member; D, Dajianshanzi Bed, Jianshangou Member; X, Xiatulaigou Member (white stippling indicates vesicles); Lujiatun Member (inferred); T, Tuchenngzi Formation. Other abbreviations: MSD, meters stratigraphic depth; SDS, sedimentary stratigraphic depth with Xiatulaigou Member lavas removed; cly, clay; mss, medium sandstone (included ashes); mcg, medium conglomerate.

Member in the core (H1-3794) is an airfall (*SI Appendix*, Fig. S4 *A* and *B*), thus permitting a direct depositional age determination and precluding the possibility of it being a reworked sample of the underlying Lujiatun Member. Our estimate of temporal duration for deposition of the lower Yixian Formation is two orders of magnitude less than the ca. 2 Myr suggested by cyclostratigraphic analysis of magnetic susceptibility in the correlative sequence at Sihetun (18) (Fig. 1), one order of magnitude less than very recent $^{40}Ar/^{39}Ar$ estimates (19), and about half as long as recent U-Pb geochronology suggests (11).

The Sanbaoyingcun outcrop sample (09.18.15-05), which is 7.9 km from core 1, and produces characteristic Lujiatun Member dinosaurs and other animals, yielded a depositional age of 125.882 +0.038/–0.057 Ma, within the uncertainty of the three samples in superposition from the core. This sample is 5 +5/–2 m directly below exposed lavas indistinguishable from the Xiatulaigou Member in the core, supporting the correlation of the basal interval of core 1 with the Lujiatun Member in outcrop Fig. 1 as shown for hypothesis 2 in Fig. 2*A*.

Zircon U-Pb LA–ICP–MS analysis of zircons from samples of matrix from two articulated specimens (IVPP 18343 and 18344: *SI Appendix*, Fig. S6) from the Sanbaoyingcun locality exhibit very similar age spectra with large peaks at ~124 Ma and ~128 Ma (with uncertainties of ca. 5 Myr), comparable to the chemical abrasion isotope dilution thermal ionization mass spectrometry (CA-ID-TIMS) age of 125.882 +0.038/–0.057 Ma for sample 09.18.15-05 from the same locality (Figs. 1 and 3). The U-Pb age of the Lujiatun matrix provides an older bound for the enclosed fossils and the U-Pb ages from the overlying strata provide the younger bound with both sets of ages lying within each other's

Downloaded from https://www.pnas.org by Paul Olsen on November 4, 2024 from IP address 67.85.115.75.

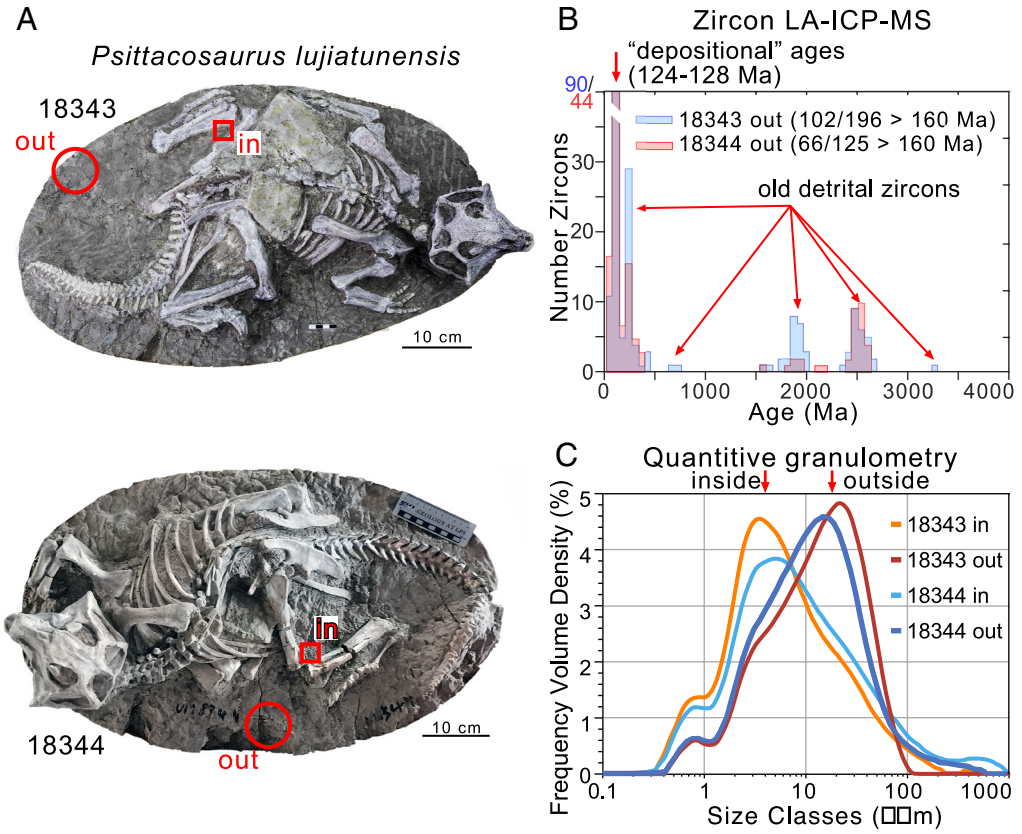


Fig. 3. *Psittacosaurus* Zircon U-Pb laser ablation (LA-ICP-MS) and quantitative diffractive granulometry data from matrix samples for two skeletons specimens of the ornithischian dinosaurs, *Psittacosaurus lujiatunensis*, from the Lujiatun Member at Sanbaoyingcun. (*A*) *P. lujiatunensis* specimens IVPP 18343 (samples P-1, P-2), and IVPP 18344, (samples P-3, P-4) showing the complete and articulated nature of the skeletons in "natural" postures. "in" and "out" refer to samples taken in each specimen, where they are proximal or distal to the skeletons on the position of the samples in being very proximal to the skeleton and out being as distal from the skeleton as possible, interpreted as being inside and outside the burrow, respectively. (*B*) Histogram of zircon dates from matrix distal from to the two dinosaur specimens (out in *B*) showing the age peaks interpreted to result from mixing between a large volcanic depositional age zircon population and detrital zircon sources ranging from the Paleozoic to Precambrian ages, presumably arising from fluvial material from the surrounding drainagearea. (*C*) Quantitative diffusive granulometry data from the two *Psittacosaurus* specimens in A showing the much finer-grained nature of the material proximal to the skeleton (in) versus more distal (out).

uncertainties. The null hypothesis that the two distributions of detrital zircons are the same cannot be rejected ($P = 0.128$), based on results of a Kolmogorov–Smirnov test (26).

Importantly, analysis of these samples reveals a wide range of detrital zircon ages ranging from Mesozoic, through Paleozoic to Archean, revealing contributions from nearby sediment sources during transport and deposition. These detrital zircon age spectra are completely unlike those from airfalls from the Jianshangou Member which lack pre-Mesozoic zircons (11). Thin-section analysis of the fossil matrix samples reveals a tuffaceous polymict sandy siltstone with rounding lithic clasts of varying lithologies (*SI Appendix*, Figs. S10–S12) and even bone clasts (*SI Appendix*, Fig. S13) that are similar to what we argue is the Lujiatun Member in core 1 (*SI Appendix*, Fig. S9). These thin-sections show that the Lujiatun Member in outcrop and core is composed of neither pyroclastic flows nor lahars but are instead simply a reworked, coarse, volcaniclastic mudstone and sandstone.

Laser diffraction particle size analysis (LDPSA) of matrix samples proximal and distal to the 3D *Psittacosaurus* museum skeletal specimens IVPP 18343 and 18344 (Fig. 3 and *SI Appendix*, Fig. S6) reveal a strong and consistent difference in grain size related to proximity to the skeletons in both fossils. Samples external to the skeleton (18343out, 18344out) have a mode between 15 and 21 μm (medium silt). Samples proximal to the skeletons (18343in, 18344in) reveal a fine-grained mode between 3.5 and 5.0 μm (clay to very fine silt).

Discussion

The Dinosaur-Bearing Lujiatun Member Was Not Deposited on a Shoreline of the Jianshangou Lake. Our stratigraphic and geochronological data do not support the hypothesis that the outcropping 3D dinosaur-bearing Lujiatun Member is a lateral equivalent shore deposit to the deep-water Jianshangou Member (Hypothesis 1 in Fig. 1). First, the drill core from Huangbanjigou shows unambiguously that the lacustrine Jianshangou Member overlies the fluvial Lujiatun Member, and therefore, these two facies cannot be time equivalents. Outcrops of the dinosaur-producing Lujiatun Member have lost the stratigraphy above, plausibly due to erosion, resulting in confusion over the true stratigraphic context of these two units until now. This stratigraphic uncertainty necessitated the use of the "upper" lava flow as a lithostratigraphic marker across the two areas. However, the upper lava flow unit in the Sihetun area is actually an intrusive sill as shown by contact relationships and the absence of vesicularity (8) and therefore cannot correlate stratigraphically to the unambiguous lavas above the outcropping Lujiatun Member. Second, our geochronological data from core and outcrop show that the entire Yixian Formation in that area was deposited in less than ~93 kyr, and previous geochronological data (*SI Appendix*, Table S4) suggesting that the Lujiatun and Jianshangou Members were lateral equivalents were too imprecise to test for synchronicity owing to the short period of deposition that we have now demonstrated. Previous studies (reviewed in ref. 27)

Downloaded from https://www.pnas.org by Paul Olsen on November 4, 2024 from IP address 67.85.115.75.

incorporating a variety of geochronological results from the Yixian Formation have suggested that the Jianshangou Member strata at Sihetun-Huangbanjigou were deposited over a time interval of one or more million years (18, 28). More recent chemical abrasion isotope dilution isotope ratio mass spectrometry (11) and $^{40}Ar/^{39}Ar$ (19) studies estimate shorter intervals of 298 and 665 kyr for the same strata. In contrast, our zircon U-Pb CA-ID-TIMS results show that the total duration recorded across the Yixian Formation at Huangbanjigou is very unlikely to be more than 100 kyr (Fig. 1). Our new results are in agreement with previous high-precision $^{40}Ar/^{39}Ar$ (19, 27) data that show that the ages of the Jianshangou and outcropping Lujiatun Members cannot be distinguished within uncertainty. Combined with evidence of superposition in core, and using Bayesian and MCMC analysis our data places extremely tight constraints on possible correlations between the outcropping Lujiatun Member, with its 3D fauna, and the lacustrine Jianshangou Member, with its flattened fauna and preserved soft tissue. In fact, the stratigraphic superposition exhibited by the Lujiatun and Jianshangou Members in Core 1 is the key observation establishing their true age relationship and supporting our hypothesis 2 (Fig. 2), where the Lujiatun Member is older than the Xiatulaigou lavas, which in turn underlie the Jianshangou Member. Nowhere is there interbedding of Lujiatun and Jianshangou facies.

Cyclicity in the Jianshangou Member is Consistent with Only Two Precession Cycles, Not Eccentricity. Previous work on the Yixian Formation in the same area at this work proposed that these Early Cretaceous lakes fluctuated at eccentricity-scale (100 s of kyr) frequencies. However, we resolve an exceedingly short depositional duration for the Jianshangou Member of less than ~93 kyr, with a corresponding accumulation rate of ~136.7 cm/kyr. This accumulation rate is one to two orders of magnitude higher than the accumulation rate previously estimated for the nearby Sihetun section of 1.70 cm/kyr (18) with a very similar stratigraphy and nearly identical thickness of the highly fossiliferous, feathered-dinosaur-producing Anjiagou Bed of the Jianshangou Member (8). With the new age model for the Huangbanjigou and correlative Sihetun sections, the implications of the finely laminated cyclic sediments at these locations can be reevaluated. Time series analysis of climate proxy data based on sedimentological facies changes [similar to "depth ranks" (29–32)], suggest that the two main fossil bearing units of the Jainshangou Member coincide with perennial chemical stratification which we attribute to greatest lake depth and therefore peak wet intervals (33), namely the Anjiagou and Hengdaozi beds (Fig. 2*B*). Using our cyclostratigraphic model, and informed by the maximum duration permissible via our age model, we demonstrate that the wet intervals are consistent with climate modulation via precession during the Early Cretaceous (Fig. 1 and *SI Appendix*, Fig. S21). Although only two cycles with deeper lake maxima are insufficient to demonstrate they were orbitally paced, the data are completely inconsistent with cyclicity in the eccentricity bands which would require a total duration of the sequence exceeding the most generous interpretation uncertainties of our analysis (49 +40/–49 kyr).

A recent U-Pb study on the Yixian Formation using a slightly different method (chemical abrasion-isotope dilution-isotope ratio mass spectrometry) (11) obtained a significantly younger age for one sample (CY17-17: 125.457 ± 0.051 Ma) for the lower Jianshangou Member (Anjiagou Bed) than both our approximately stratigraphically equivalent H1-3794 sample (125.835 ± 0.112/–0.154 Ma), and our sample 09.22.15-01 that is confidently stratigraphically well above their Jianshangou sample (*SI Appendix*, Fig. S2). Given that we, 1) produce similar ages in both Janshagou samples which are both significantly older than their sample, and 2) that their sample is from less 1.5 m below an igneous sill (Fig. S2A in ref. 11) that may have subtly affected the isotope systematics of those zircons, we regard our ages as more accurate. In addition to ages from the Lujiatun Member that are within uncertainty from ours, they also present results from a sample with a ~1.6 Myr younger age than our youngest sample, but it is from a distant locality, in a different sub-basin, that cannot be placed in relevant stratigraphic context. We regard our ages as more highly resolved and self-consistent indicating a shorter duration for the Yixian formation in the Sihuten area by a factor of about 0.5.

In addition to significant precession-related cyclicity, we also observe higher frequency peaks in the power spectra, that based on our age model, must be sub-Milankovitch in period. This sub-Milankovitch cyclicity (*SI Appendix*, Fig. S5) appears to have a reasonably consistent signal (18, 19) and may represent the kind of millennial-scale climate modulation as has been seen in high-accumulation rate, high-resolution settings elsewhere in the Late Paleozoic (34), Mesozoic (35), and Pleistocene (36), perhaps related to solar pacing. Although our average accumulation rate of 136.7 cm/kyr might appear high, it is in fact comparable to rates seen in many ancient and modern lacustrine deposits such as those of the Early Jurassic formations of the Newark Supergroup of Eastern North America (24 to 200 cm/kyr (32, 37, 38) or Quaternary strata of the African Great lakes and Lake Bosumtwi (10 to 234 cm/kyr) (39–43).

3D Lujiatun Skeletons are Preserved in Collapsed Burrows, Not Intombed by Volcanic Catastrophes. The preservation of 3D skeletons of dinosaurs, dinosaur nests, predation of dinosaurs by mammals (15), and other faunal elements in life-like poses from the outcropping Lujiatun Member has given rise to the idea they were entombed by violent volcanic eruptions, either in hot pyroclastic flows (14) or lahars (44) (volcanic debris flows). However, the Lujiatun animals are not preserved in postures typical of pyroclastic events that killed the victims of Pompeii, with "pugilistic" positions (45) or hyperflexion of the hands and feet (46) but rather are often in positions consistent with sleeping or other normal behavior (21), including predation. The numerous clusters of juveniles in nests, not dispersed, and animals in delicate sleeping positions (47, 48) with an absence of evidence of rolling, crushing, or bone breakage (49) are also completely inconsistent with being entrained in a moving lahar, which are extremely violent. These modes of preservation are instead consistent with death from sudden burrow collapse (50).

We hypothesize that if Lujiatun Member fauna were preserved in burrows, the walls of the collapsed burrows would act as sieves allowing only fine material to filter around the skeletons as the soft parts of the individuals rotted away. This phenomenon would lead to a higher proportion of finer grains in the interior of the skeletons compared to the exterior. Our LDPSA results are consistent with this "burrow sieve" hypothesis showing that matrix exterior to skeletons is three to six times coarser than material proximal to skeletal remains (Fig. 3). These data require the animals to still be fleshed out, not skeletonized, as would happen if they died exposed on the surface and scavenged (for which there is no evidence).

A cylindrical cast, or distinct burrow walls or scratch marks on burrow walls would not be evident in the case of collapsed burrows, because, apart from the entombed inhabitant, there would be little or nothing remaining to separate the sides of the structure. This is the case for collapsed tetrapod burrows of Triassic-Jurassic age (51). Burrow casts are only preserved if the burrow is filled with material, not collapsed. Burrow collapse is still a source of mortality for some extant dinosaurs, such as burrowing birds (52). Some nonavian dinosaurs did burrow, the most convincing examples being dinosaur adults and juveniles in filled, uncollapsed burrows (53), similar in size to the *Psittacosaurus* shown here. A burrow origin is consistent

Downloaded from https://www.pnas.org by Paul Olsen on November 4, 2024 from IP address 67.85.115.75.

with the abundance of articulated skeletons of multiple juveniles and species in close spatial association within the Lujiatun Formation, including an example of an articulated mammalian carnivore (*Repenomamus*) that preyed on psittacosaurs (15, 54). A plausible interpretation is that the *Psittacosaurus* were primary burrowers and other species either preyed on them or opportunistically inhabited their burrows. A similar phenomena is known to occur with modern aardvarks (55). This interpretation is supported, especially in *P. sinesis* and other Yixian species, by anatomical features such as a relatively stocky body with a robust forelimb with a humerus with large muscle attachment crests, radius, and ulna that are also robust, and short and flattened manual digits, and a relatively short but hyperflexible hind limb. These features have been noted previously as reflecting a semiaquatic habitus (56), but they are at least as consistent, if not more so, with digging behavior. Similar features have been used to infer a burrowing habitus in other dinosaurs as well (57). While it is entirely possible that local catastrophic volcanism played a role in suffocation or seismically triggered entombment, catastrophic action is not required, and essentially random burrow collapse is a parsimonious explanation for the 3D fossil preservation in the Lujiatun Member.

Furthermore, detrital zircon U-Pb LA–ICP–MS spectra from the matrix of the dinosaur skeletons found at the Sanbaoyingcun locality show that while these sediments are rich in volcanic material, they still require provenance from the surrounding areas as indicated by the presence of significant Phanerozoic and Precambrian age peaks. Although it is possible that some lithic grains could be entrained during magmatic ascent from the surrounding crust, which occurred during the eruptions of Vesuvius (58), petrographic examination (*SI Appendix*, Figs. S9–S13) of outcrop material and matrix of the skeletons, along with the detrital zircon age spectra, indicate that it is most simply interpreted as an alluvial or fluvial deposit, pedogenically modified, with a mixture of distantly transported lithic grains, recycled skeletal bits, and proximal reworked volcanic material. Together, with evidence for pedogenic homogenization, recycled bone, and the presence of adjacent conglomerates with well-rounded nonvolcanic clasts make a lahar explanation implausible. Thus, an airfall or pyroclastic flow origin is ruled out and the moniker of a catastrophic "Cretaceous Pompeii" is inappropriate.

Conclusions

The surprising result of our zircon U-Pb geochronology, astrochronology, and sedimentology is that the Jehol Biota of the flattened and 3D fauna of the Jianshangou and Lujiatun members represent in aggregate a very small amount of time (<93 kyr), are in a superpositional sequence, and cannot be lateral equivalents. These sediments cyclically sample similar if not identical ecological assemblages during three successive wet portions of climatic precession cycles, comprising one fossorial biocoenosis (Lujiatun Member) and two thanatocoenoses (Anjiagou and Huangbanjiagou beds of the Jianshangou Member). However, the preservation of the flattened and the 3D fauna are not the result of a Pompeii-like catastrophic series of volcanic processes. Rather, these sediments are millennial-scale geological snapshots in time of diverse continental communities sampled repeatedly by cyclical environmental processes and normal attrition of the communities providing the potential for inferring paleoecology in a higher-resolution way than generally possible.

Materials and Methods

Cores. The cores used in this report were collected in close proximity to important fossil localities in the Sihetun Sub-basin in the western part of the Yixian Basin. Details of the coring and recovered sequences are reported by Wang et al. (8). Samples were taken for geochronological and petrographic analysis with a diamond saw or diamond coring bit. The depth model used by Wang et al. (8) was used to construct the stratigraphic section, but the sample numbers from the core are in original depth determinations as marked on the core boxes.

Outcrop and Specimen Selection. Outcrop samples for geochronology were collected using standard field techniques, with their location recorded via an Apple iPhone. Sample 09.18.15-05 was collected directly adjacent to the drill site in a unit readily identifiable in the core (8). Samples from the *Psittacosaurus* skeletal blocks were provided by J.L. (IVPP). While these blocks were collected by local "farmers," their provenance in this case is clear.

Zircon Geochronology and Age Models. Zircons separation and U-Pb mass spectrometry via TIMS and ICP-MS were conducted using standard techniques as described by Schoene et al. (59) and Arizona LaserChron protocols, respectively. Depositional ages for each dated horizon as well as the resulting stratigraphic age model for Core 1 were calculated using a Bayesian MCMC approach described in refs. 20 and 59. More details around sample description, isotopic data, and analytical methods are available in *SI Appendix*.

Lamination Index. The Yixian lamination index (8) (Fig. 2 and *SI Appendix*, Figs. S2 and S20) is a subjective classification of sedimentary facies amenable to quantitative analysis arranged in a series along an inferred relative water depth gradient from 0 (subaerial exposure, pervasively mud-cracked) to 5 (deep water, microlaminated) similar to depth ranks as described Triassic–Jurassic strata in the eastern North American rift lacustrine sequences (29, 30, 32) but with a lower dynamic range.

Time Series Analysis and Comparison with Astronomical Solutions. Timeseries analysis of the lamination index data was conducted using the Acycle (60) software package, including multitaper spectral estimates (*SI Appendix*, Fig. S20) and TimeOpt accumulation rate estimates (*SI Appendix*, Fig. S22). The astronomical solution used was La10d (61) because it better fits highly resolved, long, early Mesozoic long lacustrine records than other solutions (32). See *SI Appendix* for details.

Granulometry. Samples for quantitative LDPSA were prepared by disaggregation and chemical cleaning followed by being run in water with Mastersizer 3000. See *SI Appendix* for details.

Data, Materials, and Software Availability. All study data are included in the article and/or supporting information.

ACKNOWLEDGMENTS. This work was supported by the Chinese Academy of Geological Sciences and National Committee of Stratigraphy of China (DD20190009) and the National Natural Science Foundation of China (91114201 and 41730317). It is a contribution to UNESCO-IUGS IGCP Project 632 and Project 4 of the CyclcoAstro project. The latter is funded by the Heising-Simons Foundation that provided partial support to P.E.O., S.K., and B.B.S. The Lamont summer intern program is thanked for the support of E.C. The Lamont Climate Center is acknowledged for support to P.E.O., C.C., B.B.S., and S.T.K. We are grateful to three reviewers whose criticisms and suggestions substantially improved the manuscript. We especially thank Bhart-Anjan Bhullar (Yale) for suggestions that anatomical features of *Psittacosaurus* that suggest it was a burrower.

Author affiliations: [a]School of Geosciences, University of the Witwatersrand, Johannesburg 2017, South Africa; [b]Department of Geosciences, Princeton University, Princeton, NJ 08544; [c]State Key Laboratory of Palaeobiology and Stratigraphy, Nanjing Institute of Geology and Palaeontology, Nanjing 210008, China; [d]Biology and Paleo Environment, Lamont-Doherty Earth Observatory of Columbia University, Palisades, NY 10964; [e]Department of Paleoichthyology and Paleoherpetology, Institute of Vertebrate Paleontology and Paleoanthropology, Chinese Academy of Sciences, Beijing 100044, China; and [f]Private address, New York, NY 10019

1. Z. Zhou, P. M. Barrett, J. Hilton, An exceptionally preserved Lower Cretaceous ecosystem. *Nature* **421**, 807–814 (2003).
2. M. Matsukawa, K. Shibata, K. Sato, X. Xing, M. G. Lockley, The early cretaceous terrestrial ecosystems of the Jehol Biota based on food-web and energy-flow models. *Biol. J. Linnean Soc.* **113**, 836–853 (2014).
3. P. J. Chen, Z. M. Dong, S. N. Zhen, An exceptionally well-preserved theropod dinosaur from the Yixian formation of China. *Nature* **391**, 147–152 (1998).
4. F. Mao, C. Zhang, C. Liu, J. Meng, Fossoriality and evolutionary development in two Cretaceous mammaliamorphs. *Nature* **592**, 577 (2021).

Downloaded from https://www.pnas.org by Paul Olsen on November 4, 2024 from IP address 67.85.115.75.

5. M. J. Benton, A colourful view of the origin of dinosaur feathers. *Nature* **604**, 630–631 (2022), 10.1038/d41586-022-01036-z.
6. M. J. Benton, Z. Zhonghe, P. J. Orr, Z. Fucheng, S. L. Kearns, The remarkable fossils from the Early Cretaceous Jehol Biota of China and how they have changed our knowledge of Mesozoic life: Presidential Address, delivered 2nd May 2008. *Proc. Geol. Assoc.* **119**, 209–228 (2008).
7. P. Chen *et al.*, Studies on the Late Mesozoic continental formations of western Liaoning. *Bull. Nanjing Inst. Geol. Palaeontol.* **1**, 22–55 (1980).
8. Y. Wang *et al.*, Stratigraphy, correlation, depositional environments, and cyclicity of the Early Cretaceous Yixian and Jurassic-Cretaceous Tuchengzi formations in the Sihetun area (NE China) based on three continuous cores. *Palaeogeogr., Palaeoclimatol., Palaeoecol.* **464**, 110–133 (2016).
9. M. M. Chang, Y. Q. Wang, Y. Wang, *The Jehol Biota* (Scientific and Technical Publishers, Beijing, China, 2003), p. 207.
10. C. S. Rogers *et al.*, The Chinese Pompeii? Death and destruction of dinosaurs in the Early Cretaceous of Lujiatun, NE China. *Palaeogeogr., Palaeoclimatol., Palaeoecol.* **427**, 89–99 (2015).
11. Y. Zhong *et al.*, High-Precision geochronological constraints on the duration of 'Dinosaurs Pompeii' and the Yixian Formation. *Natl. Sci. Rev.* **8**, nwab063 (2021).
12. T. Shao, H. Zhang, Q. Wang, Y. Liu, Y. Zhang, A mesozoic pompeii: History of the Jehol Biota's rise and fall. *Acta Geol. Sin.-Engl. Ed.* **91**, 1893–1903 (2017).
13. M. Zhang, P. Chen, Y. Wang, Y. Wang, *Jehol Biota: Biota: The Emergence of Feathered Dinosaurs, Beaked Birds and Flowering Plants* (Shanghai Scientific and Technical Publishers, Shanghai, China, 2003), p. 208.
14. B. Jiang, G. E. Harlow, K. Wohletz, Z. Zhou, J. Meng, New evidence suggests pyroclastic flows are responsible for the remarkable preservation of the Jehol Biota. *Nat. Commun.* **5**, 1–7 (2014).
15. G. Han *et al.*, An extraordinary fossil captures the struggle for existence during the Mesozoic. *Sci. Rep.* **13**, 11221 (2023).
16. S. Chang, New age constraints on the Yixian formation and its implications for the Jehol Biota. *PaleoBios* **36**, 97 (2019).
17. H. Y. He *et al.*, $^{40}Ar/^{39}Ar$ dating of Lujiatun bed (Jehol Group) in Liaoning, Northeastern China. *Geophys. Res. Lett.* **33**, L04303 (2006).
18. H. Wu *et al.*, Astrochronology for the Early Cretaceous Jehol Biota in northeastern China. *Palaeogeogr., Palaeoclimatol., Palaeoecol.* **385**, 221–228 (2013).
19. Y. Li *et al.*, Rapid preservation of Jehol Biota in Northeast China from high precision $^{40}Ar/^{39}Ar$ geochronology. *Earth Planet. Sci. Lett.* **594**, 117718 (2022).
20. C. B. Keller, B. Schoene, K. M. Samperton, A stochastic sampling approach to zircon eruption age interpretation. *Geochem. Perspect. Lett.* **8**, 31–35 (2018).
21. C. Gao, E. M. Morschhauser, D. J. Varricchio, J. Liu, B. Zhao, A second soundly sleeping dragon: New anatomical details of the Chinese troodontid *Mei* long with implications for phylogeny and taphonomy. *PLoS ONE* **7**, e45203 (2012).
22. J. Lu, A new boreopterid pterodactyloid pterosaur from the Early Cretaceous Yixian Formation of Liaoning Province, Northeastern China. *Acta Geol. Sin. (Engl. Ed.)* **84**, 241–246 (2010).
23. Q. Yang, Y. Zhao, D. Ren, An exceptionally well-preserved fossil Kalligrammatid from the Jehol Biota. *Chin. Sci. Bull.* **54**, 1732–1737 (2009).
24. L. M. Chiappe, M. Qingjin, *Birds of Stone: Chinese Avian Fossils from the Age of Dinosaurs* (Johns Hopkins University Press, Baltimore, MD, 2016).
25. A. W. Grabau, Stratigraphy of China, part 2: Mesozoic. *Bull. Geol. Surv. China* **37**, 1–771 (1928).
26. J. E. Saylor, K. E. Sundell, Quantifying comparison of large detrital geochronology data sets. *Geosphere* **12**, 203–220 (2016).
27. S. Chang, K. Q. Gao, C. F. Zhou, F. Jourdan, New chronostratigraphic constraints on the Yixian formation with implications for the Jehol Biota. *Palaeogeogr., Palaeoclimatol., Palaeoecol.* **487**, 399–406 (2017).
28. H. K. Olierook, F. Jourdan, R. E. Merle, Age of the Barremian-Aptian boundary and onset of the Cretaceous Normal Superchron. *Earth-Sci. Rev.* **197**, 102906 (2019).
29. P. E. Olsen, A 40-million-year lake record of early Mesozoic orbital climatic forcing. *Science* **234**, 842–848 (1986).
30. P. E. Olsen, D. V. Kent, Milankovitch climate forcing in the tropics of Pangea during the Late Triassic. *Palaeogeogr., Palaeoclimatol., Palaeoecol.* **122**, 1–26 (1996).
31. P. E. Olsen, D. V. Kent, Long-period Milankovitch cycles from the Late Triassic and Early Jurassic of eastern North America and their implications for the calibration of the early mesozoic time scale and the long-term behavior of the planets. *Philos. Trans. R. Soc. Lond. A* **357**, 1761–1787 (1999).
32. P. E. Olsen *et al.*, Mapping solar system chaos with the geological orrery. *Proc. Natl. Acad. Sci. U.S.A.* **116**, 10664–10673 (2019).
33. P. E. Olsen, "Tectonic, climatic, and biotic modulation of lacustrine ecosystems: Examples from the Newark Supergroup of eastern North America" in *Lacustrine Basin Exploration: Case Studies and Modern Analogs*, B. Katz, Ed. (1990), pp. 209–224.
34. R. Y. Anderson, Enhanced climate variability in the tropics: A 200 000 yr annual record of monsoon variability from Pangea's equator. *Clim. Past* **7**, 757–770 (2011).
35. D. V. Kent, G. Muttoni, P. Brack, Magnetostratigraphic confirmation of a much faster tempo for sea-level change for the Middle Triassic Latemar platform carbonates. *Earth Planet. Sci. Lett.* **228**, 369–377 (2004).
36. G. Bond *et al.*, A pervasive millennial-scale cycle in North Atlantic Holocene and glacial climates. *Science* **278**, 1257–1266 (1997).
37. P. E. Olsen, R. W. Schlische, M. S. Fedosh, "580 ky duration of the Early Jurassic flood basalt event in eastern North America estimated using Milankovitch cyclostratigraphy" in *The Continental Jurassic*, M. Morales, Ed. (New Mexico Museum of Natural History and Science, Albuquerque, NM, 1996), pp. 11–22.
38. D. V. Kent, P. E. Olsen, Early Jurassic magnetostratigraphy and paleolatitudes from the Hartford continental rift basin (eastern North America): Testing for polarity bias and abrupt polar wander in association with the central Atlantic magmatic province. *J. Geophys. Res.* **113**, B06105 (2008).
39. A. S. Cohen *et al.*, Ecological consequences of early Late Pleistocene megadroughts in tropical Africa. *Proc. Natl. Acad. Sci. U.S.A.* **104**, 16422–16427 (2007).
40. S. Lund, E. Platzman, C. Scholz, Late-Holocene paleomagnetic secular variation records from Lake Turkana, East Equatorial Africa. *Holocene* **32**, 321–333 (2022).
41. A. P. Burnett, M. J. Soreghan, C. A. Scholz, E. T. Brown, Tropical East African climate change and its relation to global climate: A record from Lake Tanganyika, Tropical East Africa, over the past 90+ kyr *Palaeogeogr., Palaeoclimatol., Palaeoecol.* **303**, 155–167 (2011).
42. R. L. Lupien *et al.*, A leaf wax biomarker record of early Pleistocene hydroclimate from West Turkana, Kenya. *Q. Sci. Rev.* **186**, 225–235 (2018).
43. T. M. Shanahan *et al.*, The formation of biogeochemical laminations in Lake Bosumtwi, Ghana, and their usefulness as indicators of past environmental changes. *J. Paleolimnol.* **40**, 339–355 (2008).
44. Q. Zhao, P. M. Barrett, D. A. Eberth, Social behaviour and mass mortality in the basal ceratopsian dinosaur *Psittacosaurus* (Early Cretaceous, People's Republic of China). *Palaeontology* **50**, 1023–1029 (2007).
45. P. Petrone, The Herculaneum victims of the 79 AD Vesuvius eruption: A review. *J. Anthropol. Sci.* **97**, 1–22 (2019).
46. G. Mastrolorenzo *et al.*, Herculaneum victims of Vesuvius in AD 79. *Nature* **410**, 769–770 (2001).
47. Q. Zhao, M. J. Benton, X. Xu, P. M. Sander, Juvenile-only clusters and behaviour of the Early Cretaceous dinosaur *Psittacosaurus*. *Acta Palaeontol. Pol.* **59**, 827–833 (2014).
48. Q. Meng, J. Liu, D. J. Varricchio, T. Huang, C. Gao, Parental care in an ornithischian dinosaur. *Nature* **431**, 145–146 (2004).
49. P. J. Baxter, Medical effects of volcanic eruptions. *Bull. Volcanol.* **52**, 532–544 (1990).
50. Y. Yang, W. Wu, P. E. Dieudonné, P. Godefroit, A new basal ornithopod dinosaur from the Lower Cretaceous of China. *PeerJ* **8**, e9832 (2020).
51. H.-D. Sues, P. E. Olsen, Stratigraphic and temporal context and faunal diversity of Permian-Jurassic continental tetrapod assemblages from the Fundy rift basin, eastern Canada. *Atl. Geol.* **51**, 139–205 (2015).
52. P. J. Seddon, Y. van Heezik, Effects of hatching order, sibling asymmetries, and nest site on survival analysis of Jackass Penguin chicks. *Auk* **108**, 548–555 (1991).
53. D. J. Varricchio, A. J. Martin, Y. Katsura, First trace and body fossil evidence of a burrowing, denning dinosaur. *Proc. R. Soc. B* **274**, 1361–1368 (2007).
54. Y. Hu, J. Meng, Y. Wang, C. Li, Large Mesozoic mammals fed on young dinosaurs. *Nature* **433**, 149–152 (2005).
55. U. Rahm, "Tubulidentates: Aardvark" in *Grzimek's Encyclopedia of Mammals. 4*, S. P. Parker, Ed. (McGraw-Hill Publishing Company, New York, NY, 1990), pp. 450–458.
56. T. L. Ford, L. D. Martin, "A semi-aquatic life habit for *Psittacosaurus*" in *New Perspectives on Horned Dinosaurs: The Royal Tyrrell Museum Ceratopsian Symposium*, M. J. Ryan, B. J. Chinnery-Allgeier, D. A. Eberth, Eds. (Indiana University Press, Bloomington, IN, 2010), pp. 328–339.
57. H. M. Avrahami, P. J. Makovicky, R. T. Tucker, L. E. Zanno, A new semi-fossorial thescelosaurine dinosaur from the Cenomanian–age Mussentuchit Member of the Cedar Mountain Formation, Utah. *Anat. Rec.*, 10.1002/ar.25505 (2024).
58. R. Cioni, R. Santacroce, A. Sbrana, Pyroclastic deposits as a guide for reconstructing the multi-stage evolution of the Somma-Vesuvius Caldera. *Bull. Volcanol.* **61**, 207–222 (1999).
59. B. Schoene *et al.*, U-Pb constraints on pulsed eruption of the Deccan Traps across the end-Cretaceous mass extinction. *Science* **363**, 862–866 (2019).
60. M. Li, L. Hinnov, L. Kump, Acycle: Time-series analysis software for paleoclimate research and education. *Comput. Geosci.* **127**, 12–22 (2019).
61. J. Laskar, A. Fienga, M. Gastineau, H. Manche, La2010: A new orbital solution for the long-term motion of the Earth. *Astron. Astrophys.* **532**, 1–15 (2011).

Downloaded from https://www.pnas.org by Paul Olsen on November 4, 2024 from IP address 67.85.115.75.

PNAS

Supporting Information for

Extremely rapid, yet non-catastrophic, preservation of the flattened-feathered and 3D dinosaurs of the Early Cretaceous of China.

Scott A. Maclennan*, Jingeng Sha*, Sean T. Kinney, Paul E. Olsen*, Clara Chang, Yanan Fang, Jun Liu, Bennett Slibeck, Elaine Chen, Blaire Schoene

*Corresponding authors: Scott A. MacLennan, Jingeng Sha, Paul E. Olsen

Emails: scott.maclennan@wits.ac.za; jgsha@nigpas.ac.cn; polsen@ldeo.columbia.edu

This PDF file includes:

Supporting text
Figures S1 to S20
Tables S1 to S4
Legends for Datasets S1 to S5
SI References

Other supporting materials for this manuscript include the following:

Datasets S1 to S5.

Supporting Information Text

1. Materials details and specimen selection

Samples were selected to span the Yixian formation as seen in the Huanbanjigou no. 1 core (referred to as Core 1 in the main text) (Figure S1 and S2) and a representation of Lujiatun Member outcrop and dinosaur specimens.

a. Cores and Samples

See Fig. S1 for locations of cores.

See Fig. S2 for sections of cores.

Sample 09.22.15-1, adjacent to core: Because of intense core breakage in the ~15 m of the core, we relied on an outcrop section directly on the hillside directly adjacent and below where the core was drilled that could be unambiguously correlated to the core.

Core sample H1-3794: Sample H1-3794 (Fig. S4A, S4B) is from the middle Jainshangou Member at core depth of 3704 cm in the Huangbanjigou no. 1 in Supplementary Fig. 4B [box 8, line 5; between 66 and 70 cm marks (cm for scale, does not denote depth)]. It is a coarse-grained, weakly graded, airfall ash interbedded with microlaminated very dark gray to black mudstone (light tan where weathered in outcrop). This core depth corresponds to a calculated stratigraphic depth of 4183 cm.

Core sample H1-8810: Sample H1-8810 (Supplementary Fig. 4C, D) is from the middle Jainshangou Member at core depth of 8810 cm in the Huangbanjigou no. 1 [box 9, line 1; at 39.5 cm mark in Fig. S4D (cm for scale, does not denote depth)]. It is fine greenish-gray and tan muddy sandstone, from an interval of mudstone to conglomerate (note lithic clasts in Fig. S4). This core depth corresponds to a calculated stratigraphic depth of 9151 cm.

b. Outcrop samples

The Lujiatun Member was sampled (09.18.15-05) on September 18, 2015 during the field trip for IGCP Project 632 (1) from Locality 5B: Sanbaoyingcun Section, Sanbaoying Village of Pan et al. (1) (see Figure SI 1, Table SI 1) where the Lujiatun Member is seen directly underlying the outcropping lavas of what we interpret to be the Xiatulaigou Member (Fig. SI 3). This is nominally the site of the two *Psittacosaurus* skeletons sampled for detrital zircons and grain size analysis (see below).

c. Dinosaurs

See Fig. S6 for images of the dinosaurs and location of samples on the specimens. Zircons form those samples are shown in Figs. S14 and S15.

2. Methods details and data

a. Thin section petrography

The thin sections (Figs. S8-S13) were prepared by Wagner Petrographic (UT, USA) from the same material as the zircon analyses and consist of standard 26 by 44 mm thin sections, 30 mm thick. A clear epoxy mount was used, and the sample was double-polished.

b. Zircon U-Pb Thermal Ionization Mass Spectrometry geochronology

Zircon separation: Zircons were separated from each sample using standard techniques. They were first sawed into small chips and then disaggregated using short runs in a SPEX 8530 ring

and puck mill. The resulting material was sieved to <500 μm and panned to obtain a rough density separation. Following panning, magnetic minerals were removed with a hand magnet and repeated runs on a Frantz isodynamic magnetic separator. A pure zircon separate was then hand-picked from the resulting heavy, nonmagnetic fraction from each sample.

Zircon U-Pb CA-TIMS: Zircons were dated at Princeton University using a modified version of chemical abrasion-isotope dilution-thermal ionization mass spectrometry (CA-ID-TIMS) (2). Zircons were first annealed at 900°C and 1 atmosphere for 60 hours. Subsequently, individual zircons were loaded into Teflon™ perfluoroalkoxy alkane (PFA) microcapsules with 100–125 μl of 29M HF and 25 μl of 30% HNO_3. The microcapsules were then loaded into a Parr dissolution vessel and held at 215°C for 12–14 hours. The resulting solutions were then discarded, and each individual zircon was repeatedly rinsed in 29 M HF, H_2O, and 6N HCl. After rinsing, approximately ~0.006 g of either the EARTHTIME 202Pb-205Pb-233U-235U double spike or ^{205}Pb-^{233}U-^{235}U single spike (in the case of sample 09-22-15-05) isotopic tracer (3, 4) and 75–100 μl of 29M HF were added to each microcapsule. The isotopic spike used in each sample is indicated in the U-Pb isotopic Dataset S1. The microcapsules were then re-loaded into a Parr dissolution vessel and held at 215°C for 60 hours for total digestion. The solutions were then dried down and dissolved in 6N HCl at 180°C for ~12 hours to convert the samples to chloride form. Uranium and Pb were purified from the dissolved sample with AG-1 X8 200–400 mesh anion exchange resin using methods modified from (5). Samples were first loaded onto 50 μl anion exchange columns in 50–75 μl of 3N HCl and rinsed dropwise to remove trace elements. Then Pb and U were eluted using 200 μl of 6N HCl and 250 μl of H_2O, respectively. Samples were dried down with a microdrop of 0.05M H_3PO_4 prior to analysis via TIMS (see Dataset SI 1).

All isotopic measurements were made on the IsotopX Phoenix TIMS at Princeton University. Lead was run as a metal and measured by peak hopping on a Daly photomultiplier. Uranium was analyzed as UO_2 and was measured statically on a series of faraday cups. Measured ratios were corrected assuming an $^{18}O/^{16}O$ of 0.00205 ± 0.00004 (2σ), corresponding to the modern atmospheric value (6). Corrections for mass dependent fractionation were done using the known ratios of $^{202}Pb/^{205}Pb$ and $^{233}U/^{235}U$ in the ET2535 isotopic tracer and assuming a $^{238}U/2^{35}U$ of 137.818 ± 0.045 (2σ), which represents the mean value of $^{238}U/^{235}U$ measured in natural zircon (7). Corrections for Pb fractionation were done cycle-by-cycle. However, the correction for U fractionation was done using the mean $^{233}U/^{235}U$ for the analysis. Daly photomultiplier dead time for Pb was monitored by running the NBS981 and NBS982 Pb isotopic standards over the range 1000 cps to 2.5 Mcps over the course of the study.

A well-known problem in the measurement of small amounts of Pb by TIMS is the effect of isobaric interferences. Known isobaric interferences include $BaPO_4$ and Tl and were corrected by measuring masses 201 and 203, assuming that they represent $^{201}BaPO_4$ and ^{203}Tl, and using the natural abundances of $^{202}BaPO_4$, $^{204}BaPO_4$, $^{205}BaPO_4$, and ^{205}Tl to correct the measurements of masses 202, 204, and 205. These corrections were minor and have no effect on our data interpretations. Additional isobaric interferences of unknown origin typically 'burn off' during the first hour of Pb analysis by TIMS. These interferences are most obvious in the measurement of ^{204}Pb, which represents the smallest ion beam. Thus, the 'burn off' results in systematic changes to the $^{204}Pb/^{205}Pb$, $^{206}Pb/^{204}Pb$, $^{207}Pb/^{204}Pb$, and $^{208}Pb/^{204}Pb$ as the reservoir for these interferences is exhausted. While the precise nature of these interferences remains unknown, the Princeton University isotope geochemistry laboratory has eliminated this problem by holding side filaments at high temperature during initial sample warm up. We anticipate that the isobaric interferences are easily volatilized molecules that coat the filament apparatus during sample warm up and that are progressively released as the apparatus warms up during the run. By holding additional filaments at high temperature, the filament apparatus heats rapidly and these molecules are volatilized and removed before the analysis begins.

A correction for common Pb (Pbc) was done by assuming that all Pbc is from laboratory contamination and using the measured ^{204}Pb and a laboratory Pbc isotopic composition to subtract the appropriate mass of Pbc from each analysis. We consider the assumption that all measured Pbc is from laboratory contamination to be robust, because the typical Pbc seen in zircon analyses (< 1 pg) is comparable to the mass of Pbc seen in procedural blanks. These procedural blanks are also used to quantify the Pbc isotopic composition at Princeton University.

For the measurements presented in this manuscript the Pbc isotopic composition was determined using all procedural blanks measured after the January 2017 adoption of the new warm up technique discussed above (n=31). The resulting Pbc isotopic composition is $^{206}Pb/^{204}Pb$ = 18.6 ± 0.6 (2σ), $^{207}Pb/^{204}Pb$ = 15.8 ± 0.4 (2σ), $^{208}Pb/^{204}Pb$ = 38.5 ± 0.8 (2σ). Overall, the correction for Pbc is negligible for the samples reported in this study due to the large radiogenic Pb (Pb*) to Pbc ratios observed in most samples (Pb*/Pbc 67-1461).

A correction for initial secular disequilibrium in the ^{238}U-^{206}Pb system due to the exclusion of Th during zircon crystallization (8) was made for each analysis using a ratio of zircon/melt partition coefficients (fThU) of 0.23 to estimate the [Th/U]Magma. This partition coefficient was empirically determined from measurements of glass and coexisting zircon rims or surfaces in a transitional tholeiitic-alkalic rhyolite erupted in Iceland (sample IETR) (9). While the tectonic setting of the volcanics dated in this study are not well constrained, the resulting [Th/U]Magma values (ca. 2 to 6) are consistent with the composition of silicic magmas erupted in rift settings (10). Regardless, the effect of this correction is negligible (<100 Ka) for the dates reported in this study.

All data reduction was done with the Tripoli and ET_Redux software packages (11) using the algorithms presented in ref. (12). The U decay constants are from ref. (13). Isotopic data is presented in the Dataset S1 as well as concordia plots. All uncertainties are reported as 2σ and represent analytical uncertainty only.

Bayesian methods for estimating individual eruption ages and the overall stratigraphic age model

The normal procedure for interpreting zircon age spectra in terms of defining an eruption age would be to calculate a weighted mean and standard error for each sample. The results from these statistical methods could then be used to estimate stratigraphic age models. The accuracy of calculating weighted means of zircon age spectra has recently come under scrutiny given that zircon crystallization timescales are not instant. See Keller et al. (14) for more discussion on this topic

For this reason, we use the Bayesian statistical approach presented by Keller et al. (14) and Schoene et al. (15). This approach consists of two separate steps: 1) calculate eruption age estimates for each of the dated samples separately, and 2) use those eruption age estimates to calculate a stratigraphic age model.

In the first step, zircon age spectra are used to calculate a distribution of eruption age estimates for each individual sample. The Bayesian prior we decided to use is a kernel density estimate of zircon saturation calculated using the observed zircon ages for each individual sample. This methodology directly follows that presented by (14).

The second step of the process follows the procedure presented by Schoene et al. (15) and uses the estimated eruption age distributions from the first step, as well as the constraint of stratigraphic superposition to produce an age-depth model using a Markov chain Monte Carlo approach.

These procedures result in deposition age distributions throughout the stratigraphy. The duration distribution discussed in the main text was calculated by calculating the difference between the uppermost and lowermost age distributions in the stratigraphy.

The Chron.jl code was used to calculate the individual eruption age estimates from the first step, as well as the final age-depth model for the second step (https://github.com/brenhinkeller/Chron.jl).

The TIMS U-Pb data are available in dataset S1 entitled “Dataset_SI_1_TIMS_U-Pb_zircon_data_table.xlsx”

c. U-Pb geochronologic analyses of detrital zircon (Nu HR ICPMS)

Subsamples of the *Psittacosaurus* dinosaur skeleton matrix (18343out and IVPP 18344out) were processed for detrital zircons to test the hypothesis that the matrix was a reworked volcanoclastic unit as opposed to a pristine lahar, air fall, or ash flow. Data tables are in dataset

Zircon preparation: Zircon separation for detrital analysis was undertaken at the University of Arizona. Zircon crystal extraction from samples was undertaken by the traditional methods of

crushing and grinding, followed by separation with a Wilfley table, heavy liquids, and a Frantz magnetic separator. Samples are processed such that all zircons are retained in the final heavy mineral fraction. A large split of these grains (generally thousands of grains) is incorporated into a 1" epoxy mount together with fragments of the Sri Lanka zircon standard (SL) and zircons from the Duluth gabbro (FC-1). The mounts are sanded down to a depth of ~20 microns, polished, imaged, and cleaned prior to isotopic analysis.

LA-ICPMS analysis: U-Pb geochronology of zircons was conducted by laser ablation multicollector inductively coupled plasma mass spectrometry (LA-MC-ICPMS) at the Arizona LaserChron Center (16, 17) [See Datasets S2 and S3 (Dataset_SI_2_IVPP_18343_data table.xls and Dataset_SI_2_IVPP_18344_data table.xls)].

The analyses involve ablation of zircon with a Photon Machines Analyte G2 excimer laser using a spot diameter of 30 microns. The ablated material is carried in helium into the plasma source of a Nu HR ICPMS, which is equipped with a flight tube of sufficient width that U, Th, and Pb isotopes are measured simultaneously. All measurements are made in static mode, using Faraday detectors with 3x1011 ohm resistors for ^{238}U, ^{232}Th, ^{208}Pb-^{206}Pb, and discrete dynode ion counters for ^{204}Pb and ^{202}Hg. Ion yields are ~0.8 mv per ppm. Each analysis consists of one 15-second integration on peaks with the laser off (for backgrounds), 15 one-second integrations with the laser firing, and a 30 second delay to purge the previous sample and prepare for the next analysis. The ablation pit is ~15 microns in depth.

For each analysis, the errors in determining ^{206}Pb/^{238}U and ^{206}Pb/^{204}Pb result in a measurement error of ~1-2% (at 2-sigma level) in the ^{206}Pb/^{238}U age. The errors in measurement of ^{206}Pb/^{207}Pb and ^{206}Pb/^{204}Pb also result in ~1-2% (at 2-sigma level) uncertainty in age for grains that are >1.0 Ga, but are substantially larger for younger grains due to low intensity of the 207Pb signal. For most analyses, the cross-over in precision of ^{206}Pb/^{238}U and ^{206}Pb/^{207}Pb ages occurs at ~1.0 Ga.

^{204}Hg interference with ^{204}Pb is accounted for measurement of ^{202}Hg during laser ablation and subtraction of ^{204}Hg according to the natural ^{202}Hg/^{204}Hg of 4.35. This Hg is correction is not significant for most analyses because our Hg backgrounds are low (generally ~150 cps at mass 204).

Common Pb correction is accomplished by using the Hg-corrected ^{204}Pb and assuming an initial Pb composition from Stacey and Kramers (1975) (18). Uncertainties of 1.5 for ^{206}Pb/^{204}Pb and 0.3 for ^{207}Pb/^{204}Pb are applied to these compositional values based on the variation in Pb isotopic composition in modern crystal rocks.

Inter-element fractionation of Pb/U is generally ~5%, whereas apparent fractionation of Pb isotopes is generally <0.2%. In-run analysis of fragments of a large zircon crystal (generally every fifth measurement) with known age of 563.5 ± 3.2 Ma (2-sigma error) is used to correct for this fractionation. The uncertainty resulting from the calibration correction is generally 1-2% (2-sigma) for both ^{206}Pb/^{207}Pb and ^{206}Pb/^{238}U ages.

Concentrations of U and Th are calibrated relative to our Sri Lanka zircon, which contains ~518 ppm of U and 68 ppm Th.

The analytical data are reported in Datasets S3 and 4 (Dataset_SI_2_IVPP_18343_data_table.xlsx ; Dataset_SI_3_IVPP_18344_data_table.xlsx). Uncertainties shown in these tables are at the 1-sigma level, and include only measurement errors. Analyses that are >20% discordant (by comparison of ^{206}Pb/^{238}U and ^{206}Pb/^{207}Pb ages) or >5% reverse discordant are not considered further. Summary data are reported in Table S3.

e. Time series analysis and astrochronology

Core Depth Series: Data for the timeseries analysis are in Dataset S4 (Dataset_SI_4 haungbanjigou1_jianshangou_stratigraphic_data.xlsx) which contains the original lamination index depth rank series as marked on the core boxes, which was corrected to stratigraphic depth using polynomial regression with the driller's depth as marked on insertions into the boxes at the bottom of each core barrel run (Figure 2, SI2). The original depths and procedures are given by Wang et al. (19). Driller's depth is more accurate than core box depth because the former is based on the amount of drill string actually in the hole vs core box depth

which is measured with a tape measure on the boxed core, the latter not accounting for core loss and damage. Most modifications needed were for the upper parts of the core where there was considerable core loss.

Time Series Analysis: For time series analysis we spliced the outcrop section of the Huangbanjigou Bed and the core section of the Hengdaozi Bed (joined at their mutual boundary) to compensate for the considerable crushing and some jumbling of the core due to weathering in stratigraphy around the Huangbanjigou Bed as described in ref. (19). The interval in the core comprised of the extrusive volcanic (lava) Xiatulaigou Member was removed prior to time series analysis. The composite section with lamination index, color, and qualitative grainsize is available in Datafile S4. For definitions of classifications regarding color, grain size and depth rank see reference (19).

We show that the duration the Jianshangou Member is very short. Comparing the extremes of our age models, it is no more than 100 kyr with an accumulation rate of 47.4 cm/kyr (Lower bound on accumulation rate) and 7 kyr with an accumulation rate of 725.9 cm/kyr (upper bound on accumulation rate). This range is one to two orders of magnitude higher than the accumulation rate estimated for the nearby Sihetun section of 1.70 cm/kyr (20) based on much weaker geochronological constraints but with a very similar stratigraphy and nearly identical thickness of the highly fossiliferous, feathered-dinosaur-producing, Anjiagou Bed of the Jianshangou Member (19). The median of our preferred 3-age model, 136.7 cm/ky, is nearly two orders of magnitude higher than previous estimates and suggests the entire Yixian Formation in the Sihetun-Huangbanjigou area represents less than 100 kyr, a snapshot of geological time.

Time series analysis of the Huangbanjigou and correlative Sihetun sections suggests that the main fossil bearing units comprise peak wet intervals in three individual climatic precession cycles spanning about 60 kyr total. Power spectra of color, grain size, and lamination index (Fig. 2 in the main text and SI Fig. S21) show similar single peaks in thickness periods compared to each other and to the Huangbanjigou and Sihetun cores in the higher frequency range (1-2 m), both in terms of our analysis and previous work (Fig. S21). At Huangbanjigou the only prominent peaks average about 29.4 m/cycle. With the preferred accumulation rate of 136.7 cm / kyr, this peak would correspond to a period of 21.5 kyr / cycle, falling well within the climatic precession band for Early Cretaceous time (126 Ma).

Filtering the Huangbanjigou core and outcrop interval comprised of the Anjiagou through overlying undivided Yixian Formation in the Huangbanjiagou no. 1 core at its most prominent frequency of 0.0486±0.010 cycles/m yields a curve that can be matched closely by the climatic precession index of the La10d solution from 125.779 - 127.820 Ma. The exact phase and hence exact ages cannot be realistically determined by the solution, although the period of the cycle is more robust and closely comparable to the period based independently by the U-Pb data from the core (23.4 for La10d vs 21.5 kyr for our U-Pb rate).

Attempts at fitting the Huangbanjiagou data to a precession-eccentricity model using the TimeOpt method (21) executed in Acycle (22) centered on 126 Ma failed to find a good fit, consistent with the U-Pb time constraints, because of the very short duration of the Huangbanjiagou section. However, assuming an accumulation rate based on our new U-Pb data, and limiting the range of accumulation rate to between 50 and 200 cm/kyr TimeOpt yields an, accumulation rate of 128.15 cm/kyr (Fig. S22), very close to our empirical rate of 136.7 cm/kyr from our preferred age model. Therefore, the higher frequency peaks in the power spectra must therefore be sub-Milankovitch in period and eccentricity modulation of the section cannot be observed. This seemingly consistent (20, 23) sub-Milankovitch cyclicity may be similar to that seen in high-accumulation rate settings elsewhere in the late Paleozoic (24), Mesozoic (25) and Pleistocene (26), perhaps related to solar pacing.

While the total uncertainty of the new ages permits as little as 10 kyr and as much 163 kyr or even zero time for the duration of the Yixian Formation in this area, our preferred age model results in excellent agreement between the observed lithological cyclicity and Early Cretaceous climatic precession and is the most parsimonious hypothesis of accumulation rate and cyclicity (Fig. S21). Based on the preceding analysis, the three climatic precession peaks in the filtered sequence fall close to the principal fossil bearing intervals of the Yixian formation, which produced the famous Jehol Biota in the Sihuten-Huangbanjiagou-Lujiatun area: the middle of the

Lujiatun Member, the Anjiagou Bed of the Jianshangou Member, and the upper Hengdaozi Bed of the Jianshangou Member.

f. Quantitative granulometry
Two samples for quantitative granulometry each were selected from the *Psittacosaurus* specimens IVPP 18343 (18343in and 18343out), and IVPP 18344 (18344in and 18344out), with 18343in and 18344in being within the inner thigh region adjacent to the femur, and 18343out and 18344out being as distal from the skeleton as possible, interpreted as being outside and inside possible burrows, respectively. See Dataset_S5 (Dataset_SI_5_granulometry_data.xlsx).

Disaggregation and removal of organic material, pyrite, and carbonate cement: About 3 to 5 grams of fossil matrix material was processed for laser granulometry analysis. Prior to laser granulometry analysis the fossil matrix material needed to be disaggregated and organic material, pyrite and carbonate cement needed to be removed. The 3-5g of rock sample material was covered with 30% H2O2, warmed on a 50°C hot plate for 1 hour and sat at room temperature overnight. This process disaggregated the rock into individual grains. Oxidation of pyrite forms H_2SO_4 that dissolved the carbonate cement. Thin section analysis indicated that the carbonate was restricted to matrix cement, and no carbonate clasts were present that would be dissolved.

Laser granulometry sample preparation: About 3 to 5 grams of fossil matrix material was processed for laser granulometry analysis. Prior to laser granulometry analysis the fossil matrix material needed to be disaggregated and organic material, pyrite and carbonate cement needed to be removed. The 3-5g of rock sample material was covered with 30% H2O2, warmed on a 50°C hot plate for 1 hour and sat at room temperature overnight. This process disaggregated the rock into individual grains. Oxidation of pyrite forms H_2SO_4 that dissolved the carbonate cement. The coarse fraction was inspected using light microscopy to verify total disaggregation. Samples were rinsed and centrifuged three times with DI water. In order to remove charcoal, saturated zinc chloride solution was added to each sample and centrifuged to float out charcoal and other recalcitrant organics, which were pipetted off. This process was repeated until there was no visible charcoal left in the sample. Samples were rinsed and centrifuged three times with DI water.

Laser diffraction grain size analysis: Samples were run by Particle Technology Labs, Downers Grove, Illinois. Samples were run in water with Mastersizer 3000, with a Hydro MV accessory. The particle refractive index was 1.520, with a General-Purpose Model, normal sensitivity. Samples were sonified before and during the sample run to reduce clumping.

Fig. S1

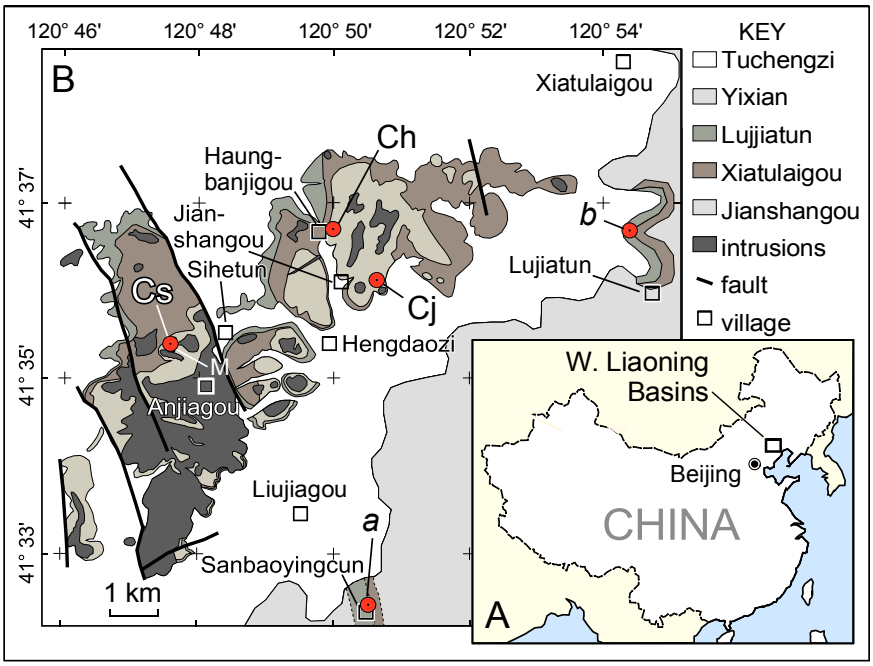


Fig. S1. Location of cores and outcrops. Map of the Sihetun-Huangbanjiagou-Lujiatun-Sanbaoyingcun area, Liaoning Province, China [from main text Figure 1, modified from (19)]. A, Index map showing location of study area in China. B, Geologic map showing a, location of Sanbaoyingcun sample; b, type section of the Lujiatun Member (1); key localities: Ch, is Huangbanjiagou no. (Core 1 in main text); Cj, is the Jianshangou no. 1 core; Cs, is Sihetun no. 1 (Core 2 in main text). These cores are described in detail in ref. (19) and shown in Fig. S2.

Fig. S2

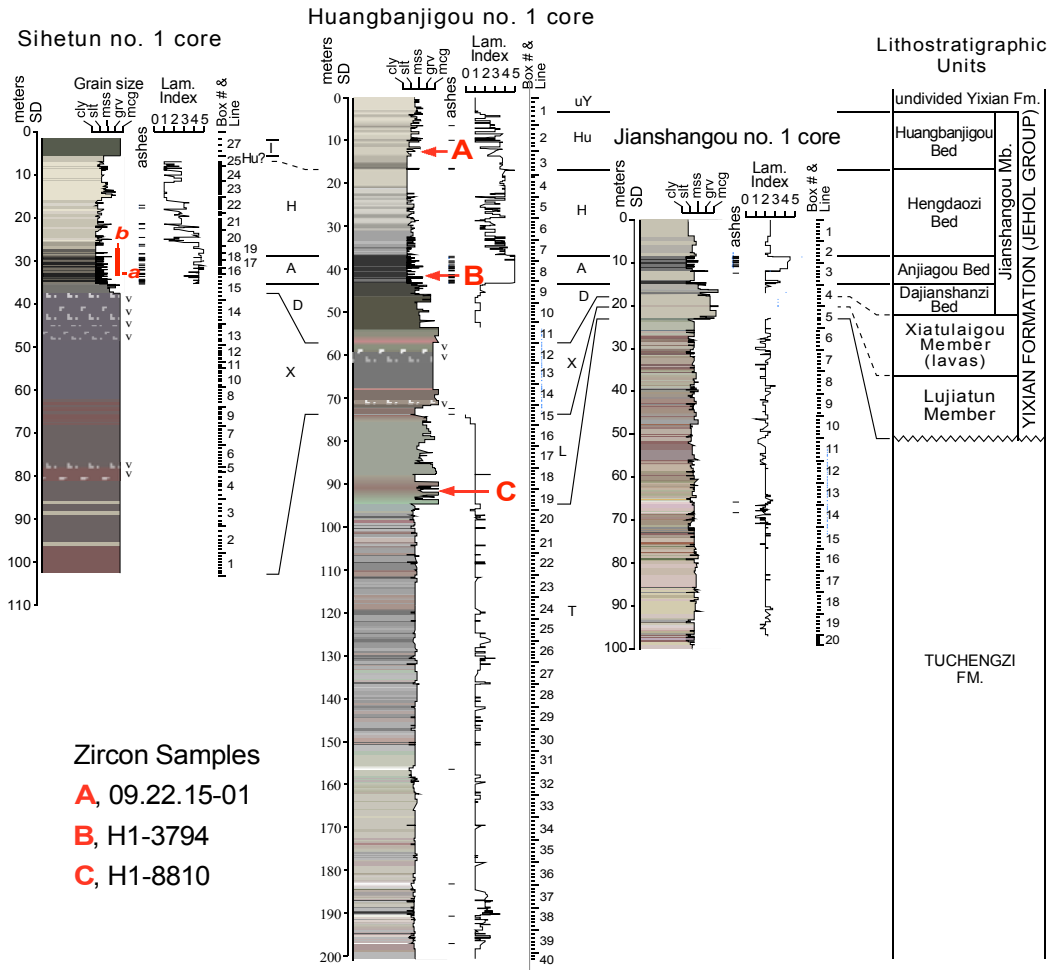


Fig. S2. Cores from the Yixian Formation from the Sihutun – Huangbanjigou area showing location of samples (see Fig. S1 and Table S1 for locations). Adapted from Wang et al. (19). A, B, and C are the samples analyzed from the core and adjacent outcrop (A, 09.22.15-1) in this paper. Cores are correlated at the base of the Anjiagou Member and to the same depth scale. Abbreviations are: A, Anjiagou Member; D, Dajianshanzi Bed; H, Hengdaozi Bed; Hu, Huangbanjigou Bed; I, Igneous Intrusion; L, Lujiatun Member; T, Tuchengzi Formation; v, vesicles in extrusive igneous rock of the Xiatulaigou Member; X, Xiatulaigou Member; Lam. Index, lamination index; a, tie interval between type section of Anjiagou Bed and Sihetun no. 1 core; b, correlative interval between Sihetun no. 1 core and type section.

Fig. S3

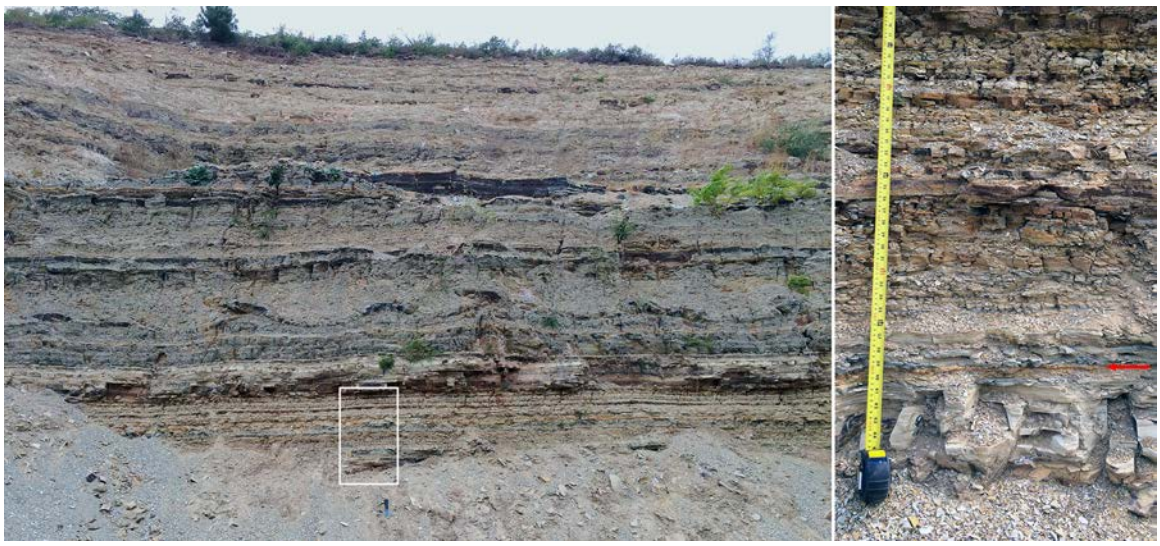


Fig. S3. Sample 09.22.15-1, adjacent to core. Left, overview of exposure; Huangbanjigou core was drilled on top of this hill; white inset shows position of close up on right [hammer head (blue) is 18 cm]. Right, close up of exposure producing sample; red arrow is sampled ash 09.22.15-1 (red arrow); tape measure is in inches (right) and centimeters (left).

Fig. S4



Fig. S4. Samples H1-3794 (A, B) and H1-8810 (C, D) from Huangbanjigou no. 1 (scale in centimeters); sample number corresponds to core box depth. A, Box 8 of Huangbanjigou no. 1, white brackets show position of sample H1-3794 in B. B, Detail of coarse-grained airfall comprising sample H1-3794. C, Box 19 of Huangbanjigou no. 1, white brackets show position of sample H1-8810 in D.

Fig. S5

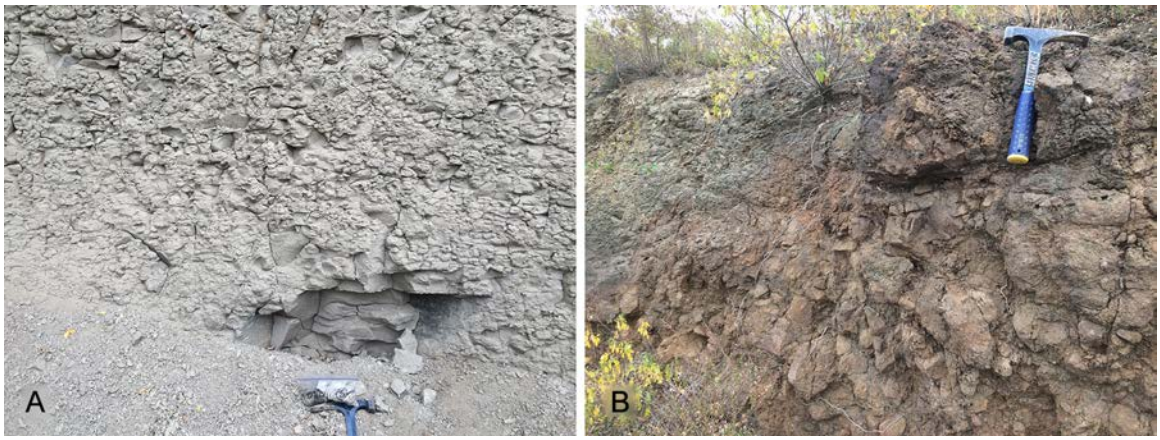


Fig. S5. Exposures of the massive, volcanoclastic Lujiatun Member (A) and overlying (extrusive) vesicular lavas of what we interpret to be the Xiatulaigou Member lavas at the Sanbaoying Village (Sanbaoyingcun) outcrop of ref. (1). Bag containing our sample 09.18.15-05 in in foreground in A. Hammer head is 18 cm.

Fig. S6

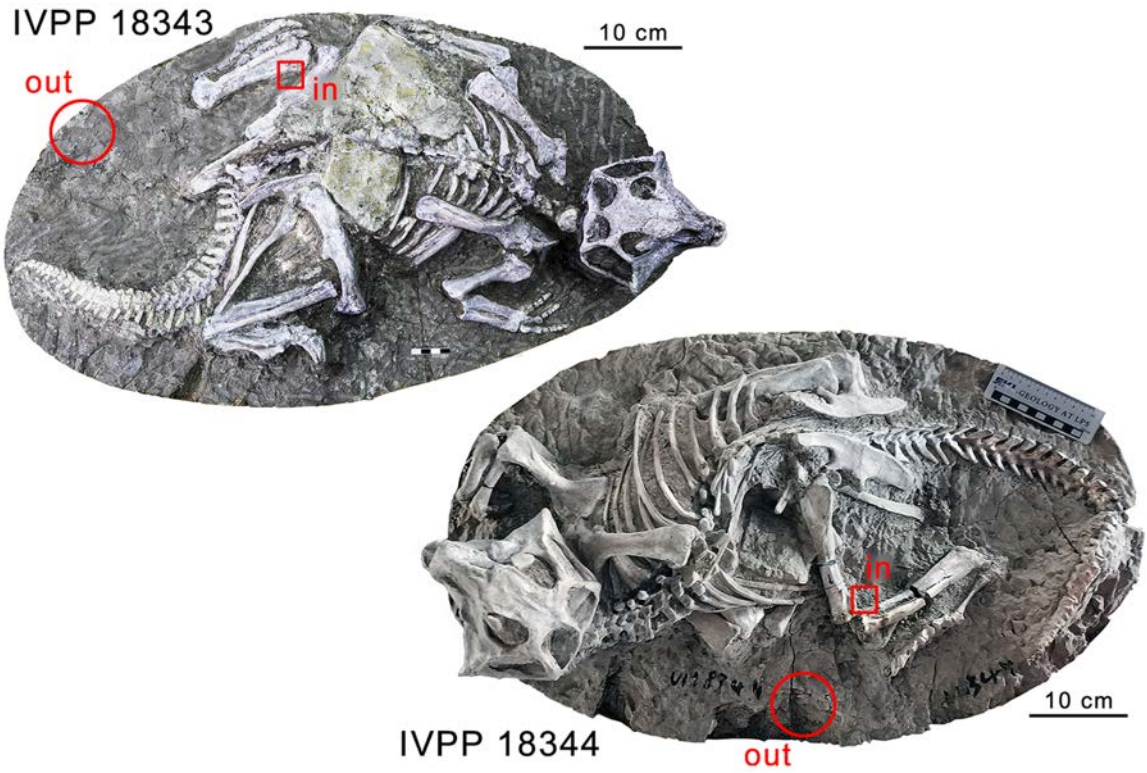


Fig S6. The two *Psittacosaurus* sp. specimens sampled for detrital zircons and for quantitative granulometry from Sanbaoyingcun. Samples are 18343out and 18344out for detrital zircons and granulometry and 18343in and 18344in for granulometry (see section 2).

Fig. S7.

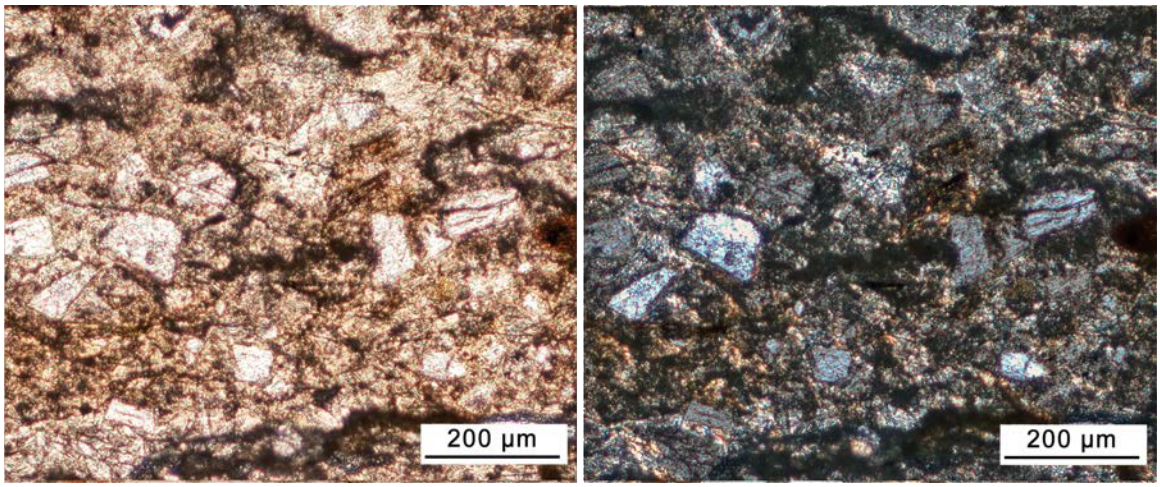


Fig. S7. Thin Section of 09.22.15-01: left, plain transmitted light; right, crossed polarized light. The sample is an airfall ash comprised of sand - and silt-sized euhedral but altered plagioclase, mica, and quartz in a clay matrix, most simply interpreted as altered glass. The sample is from outcrop and is cracked parallel to bedding, with the cracks filled with clay, a feature typical of the airfalls in the Yixan Formation. This is a surface sample and exhibits more alteration than H1-3794 from core, below.

Fig. S8.

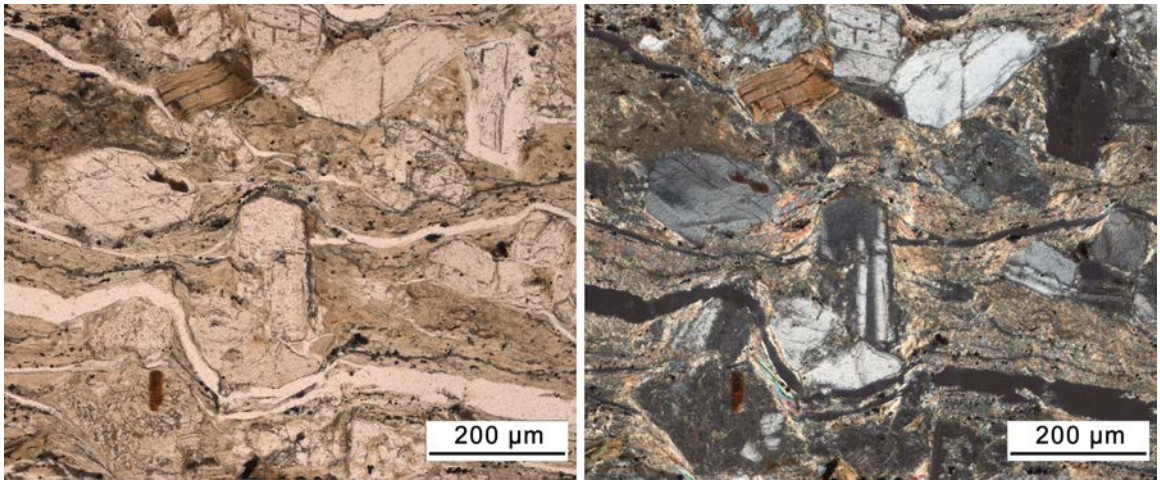


Fig. S8. Thin section of H1-3794: left, plain transmitted light; right, crossed polarized light. The sample is from the Huangbanjigou core and is a graded airfall ash comprised of sand - and silt-sized euhedral but altered plagioclase, mica, and quartz in a clay matrix, most simply interpreted as altered glass. The sample is cracked parallel to bedding as in 09-22-15-01, but in this case, the cracks formed due to wetting and drying after coring were are air-filled (now epoxy-filled).

Fig. S9.

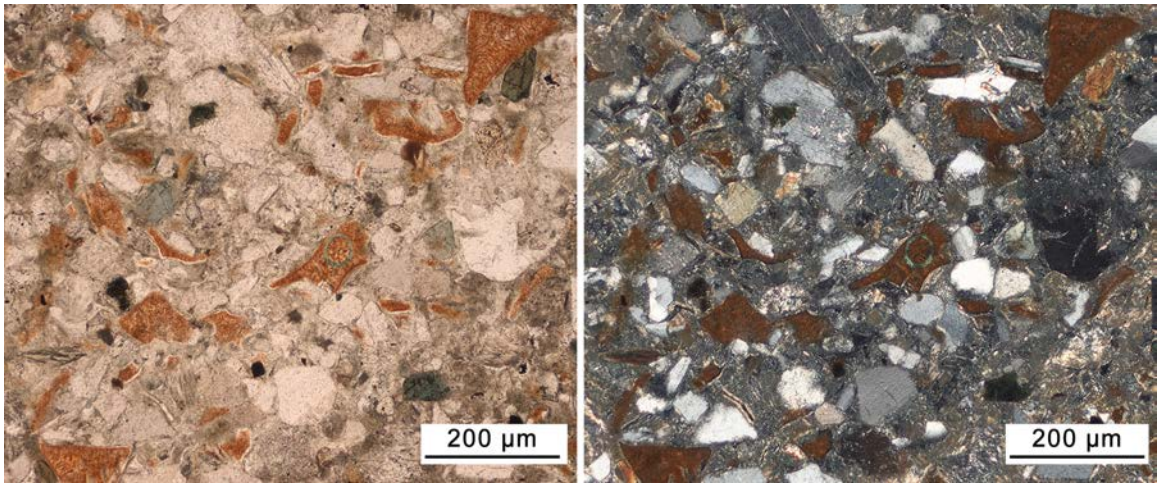


Fig. S9. Thin section of H1-8810: left, plain transmitted light; right, crossed polarized light. The sample is from the Huangbanjigou core and is volcaniclastic in origin. It is a sandy, coarse volcaniclastic mudstone with polymict silt and sand sized grains including many clasts of rounded igneous and other rocks, as well as orange altered glass. A larger complex, rounded lithic clast can be seen on the right, middle.

Fig. S10.

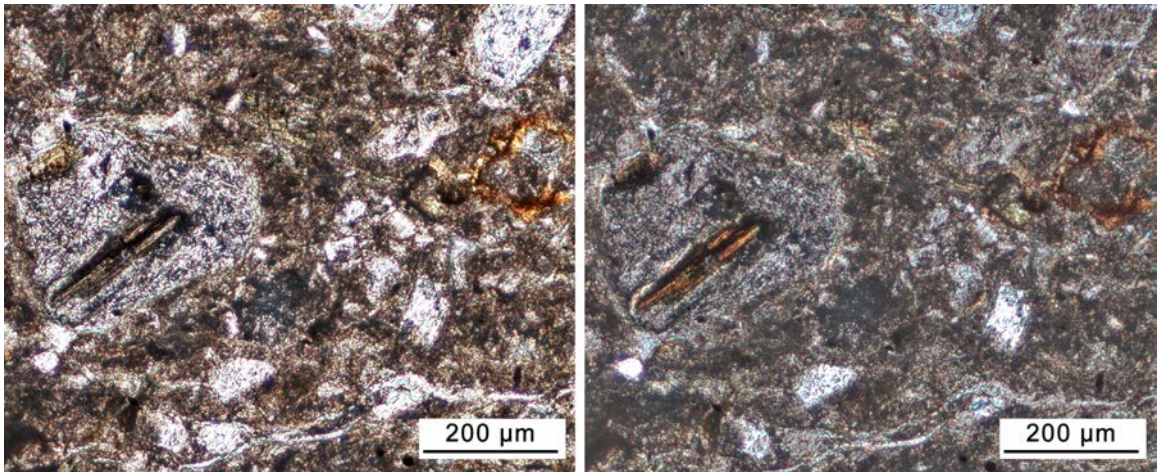


Fig. S10. Thin section of 09.18.15-05: left, plain transmitted light; right, crossed polarized light. This sample is from outcrop at Sanbaoyingcun. As with H1-8810, the sample is a sandy, coarse volcaniclastic mudstone with polymict silt and sand-sized grains including many clasts of rounded igneous and other rocks, as well as altered glass. A larger complex, rounded lithic clast can be seen on the left, middle. This sample is more weathered than H1-8810, which was sampled from core.

Fig. S11.

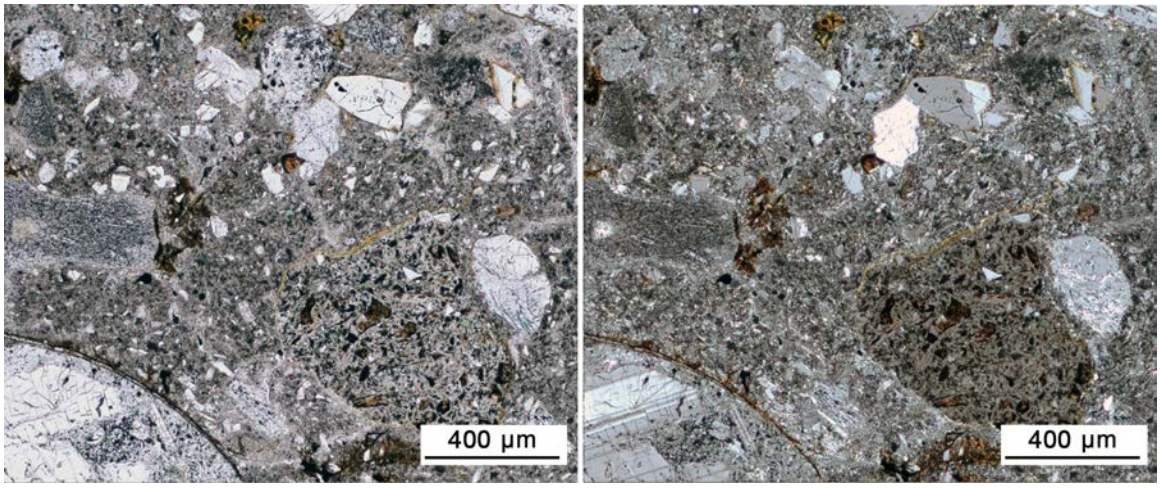


Fig. S11. Thin section of IVPP 18343: left, plain transmitted light; right, crossed polarized light. This sample is from the outer matrix that hosts a *Psittacosaurus* skeleton (Fig. S6). As with H1-8810 and 09.18.15.05, the sample is a sandy, coarse mudstone with polymict granule-, silt- and sand-sized grains including many clasts of rounded igneous and other rocks, as well as altered glass. A tabular, micaceous, clastic, mudstone lithic last is visible on the right middle. And a rounded volcanoclastic (?) lithic clast is in the lower right quadrant. Many other rounded clasts are visible.

Fi. S12.

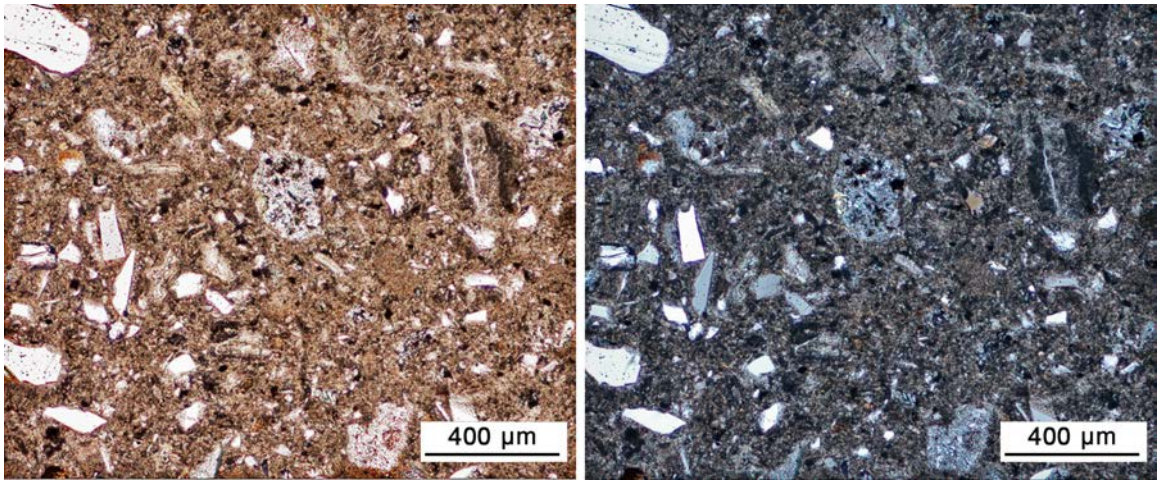


Fig. S12. Thin section of IVPP 18344: left, plain transmitted light; right, crossed polarized light. This sample is from the outer matrix of material that contains a *Psittacosaurus* skeleton (Fig. S6). As with H1-8810, 09.18.15.05, and IVPP 18343 the sample is a sandy, coarse mudstone with polymict lithic, silt and sand sized grains including many clasts of rounded igneous and other rocks, as well as altered glass. Rounded, sand-sized, igneous, lithic clasts are present, some of them, clear lithic rock fragments. This sample has more angular fragments than IVPP 18344.

Fig. S13.

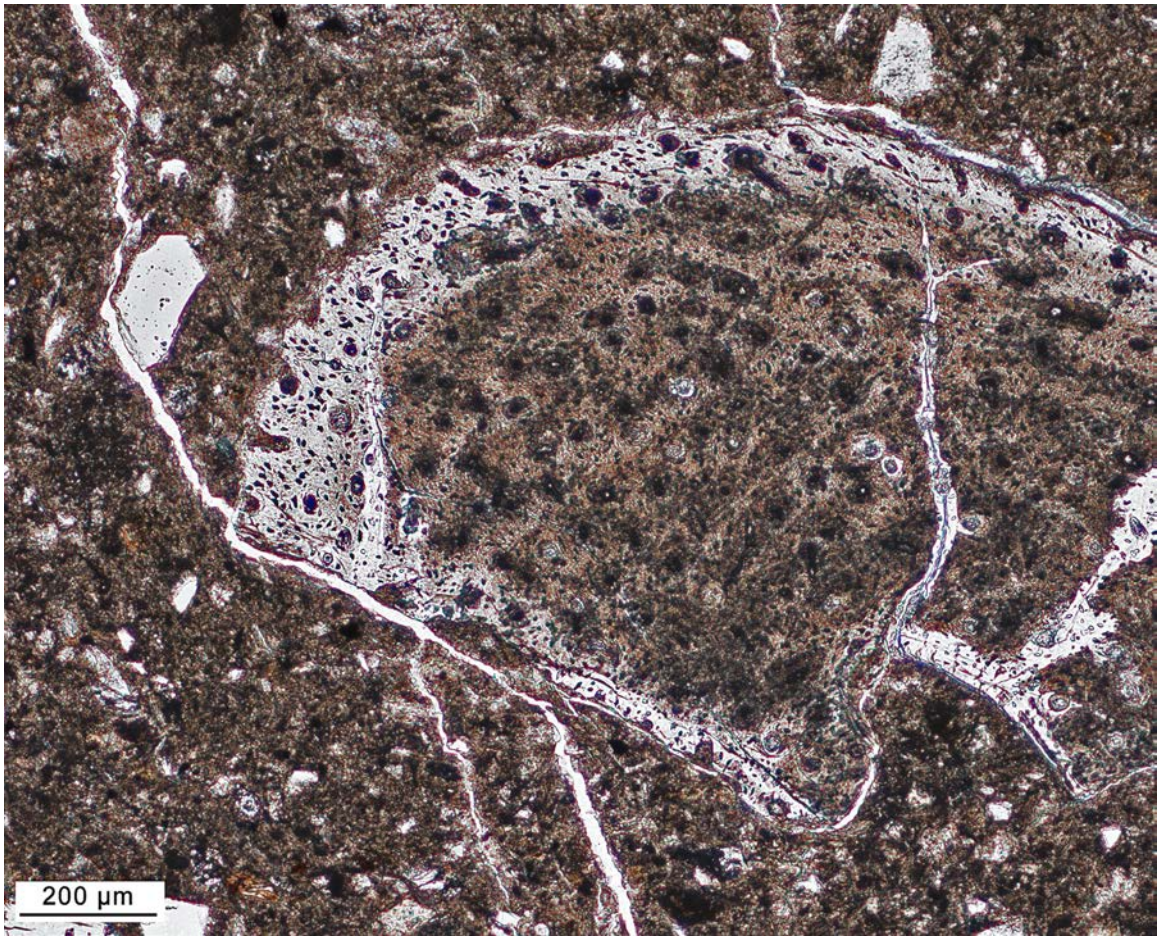


Fig. S13. Eroded bone fragment in thin section of IVPP 18344, outer matrix; same thin section as Fig. S12. In plain transmitted light. This sample is from outer matrix containing a *Psittacosaurus* skeleton (Figure S6). Bone has a clear haversian system with concentrically arranged osteocytes and is most simply interpreted as a small clast of plausibly dinosaur bone, unrelated to the articulated *Psittacosaurus* skeleton (Fig. S6). However, it lacks apomorphies and is indeterminate. It is difficult to imagine how it could be incorporated into a pyroclastic flow or a lahar. Most parsimoniously, it is simply part of the reworked, coarse, volcaniclastic mudstone.

Fig. S14.

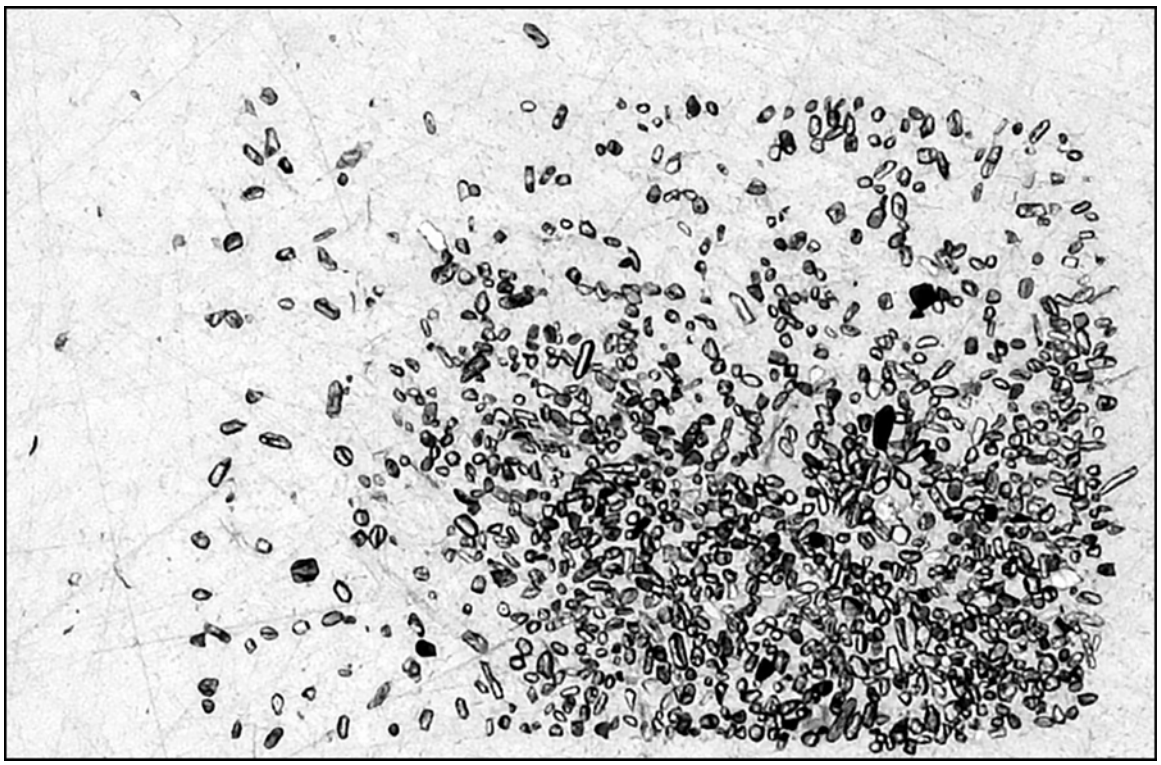


Fig. S14. Epoxy mount of heavy mineral fraction of the outer matrix sample from specimen IVPP 18343. This material was sampled from the host sediment from the *Psittacosaurus lujiatunensis* fossil specimen. Zircons from this heavy mineral fraction were analyzed for their U-Pb age via LA-ICP-MS.

Fig. S 15.

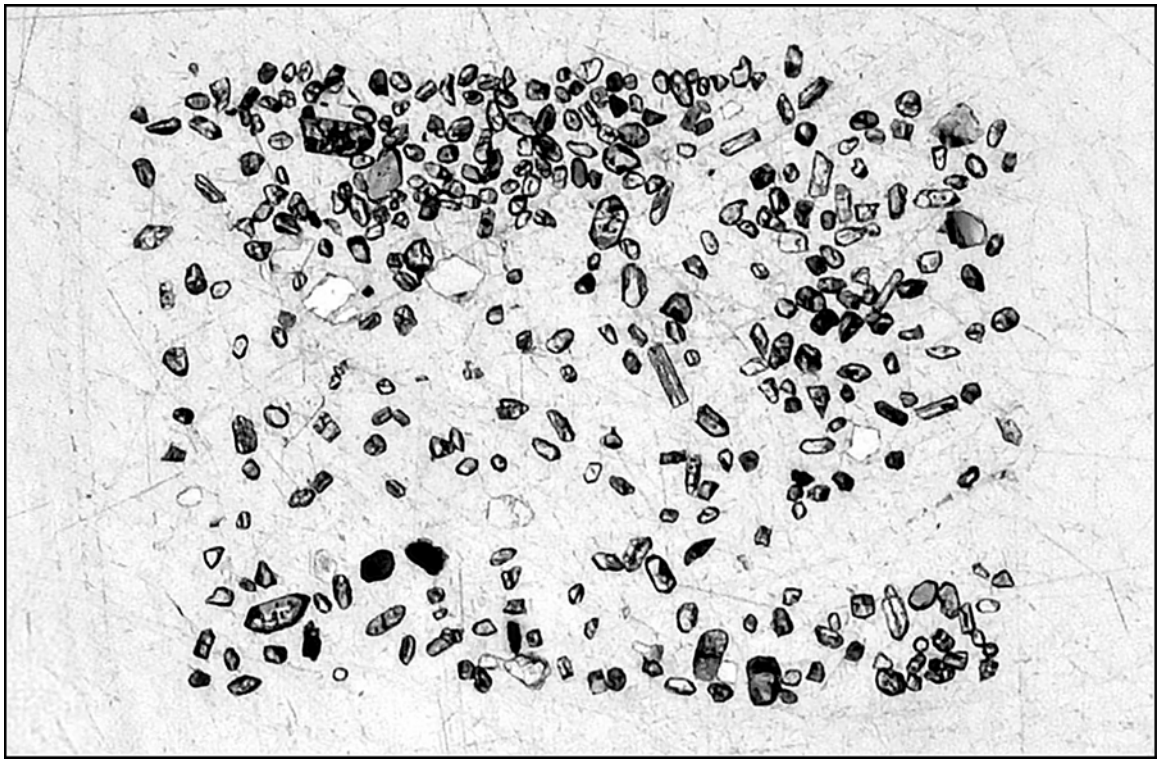


Fig. S15. Epoxy mount of heavy mineral fraction of the outer matrix sample from specimen IVPP 18344. This material was sampled from the host sediment from the *Psittacosaurus lujiatunensis* fossil specimen. Zircons from this heaby mineral fraction were analysed for their U-Pb age via LA-ICP-MS.

Fig. S16.

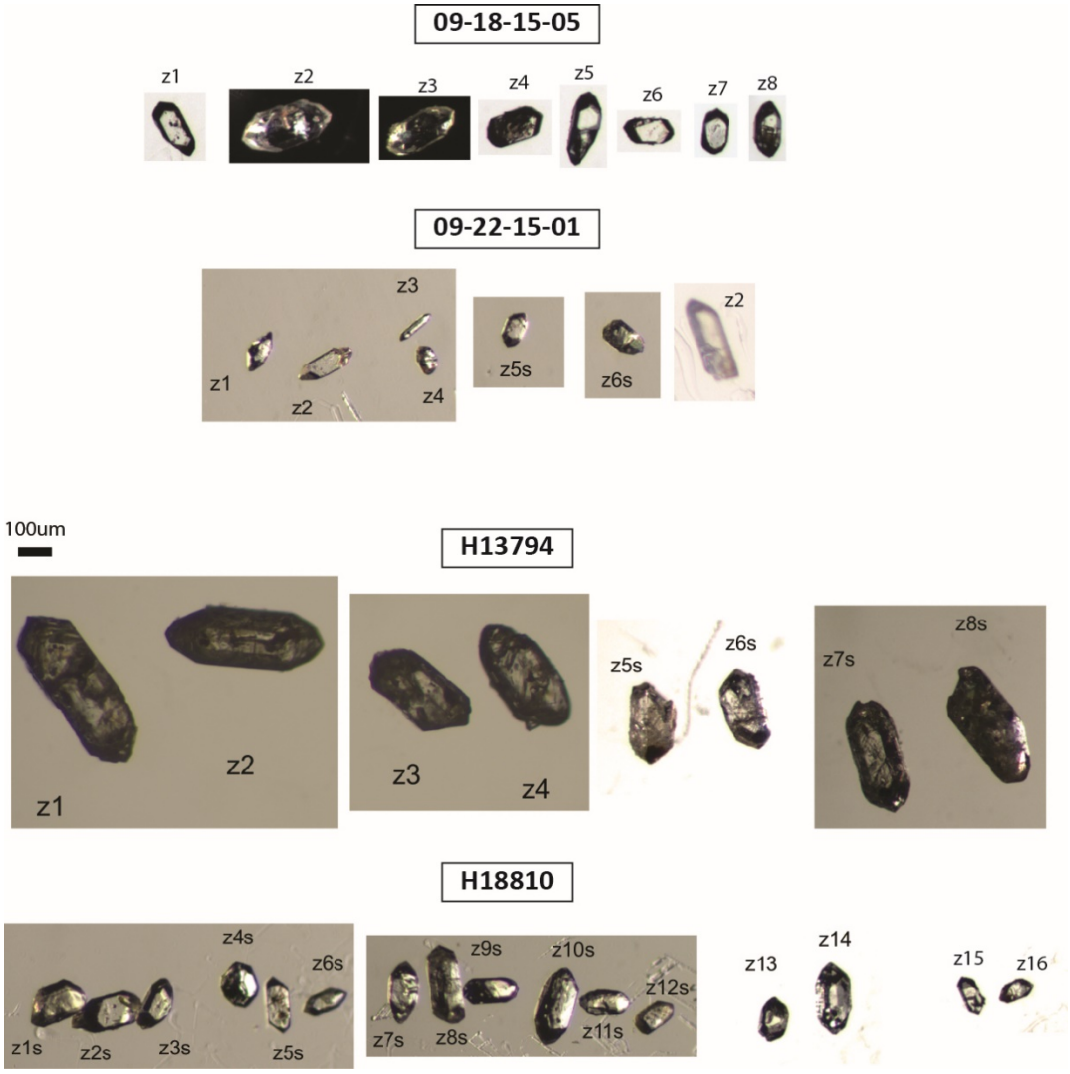


Fig. S16. zircons selected for CA-TIMS analysis.

Fig. S17.

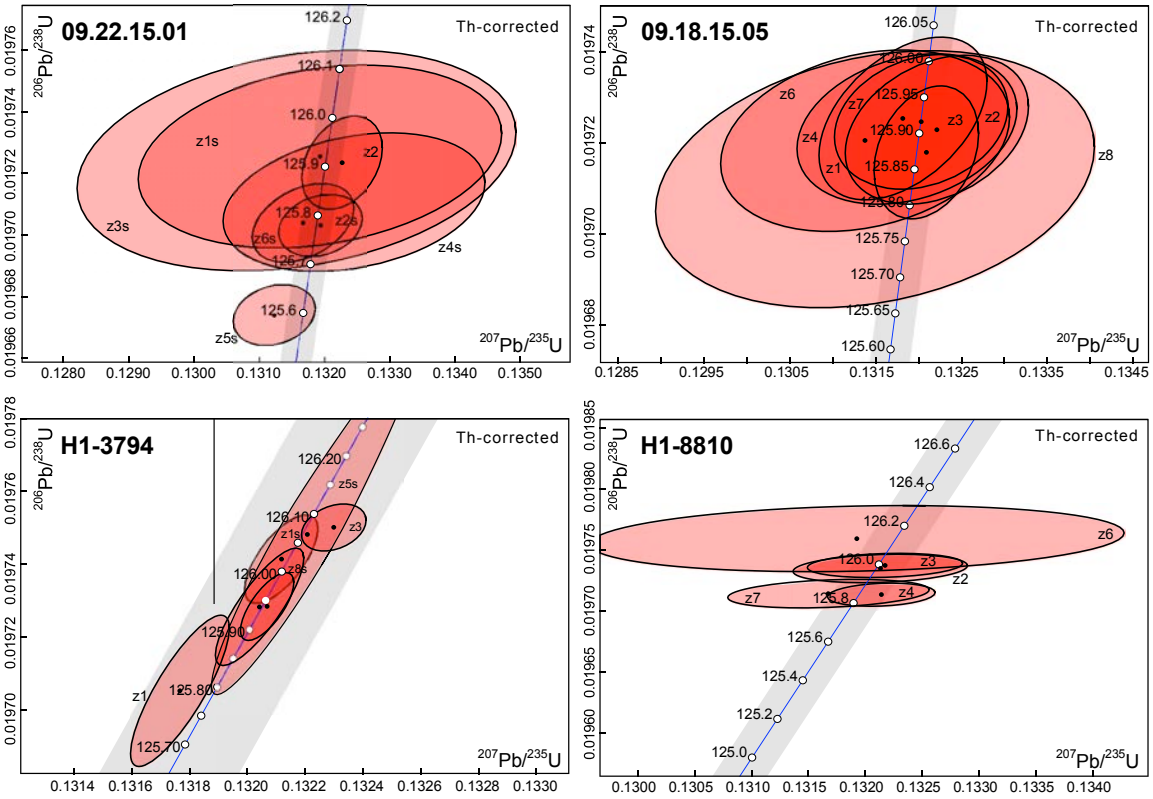


Fig. S17. Concordia diagrams for the CA-TIMS data.

Fig. S18,

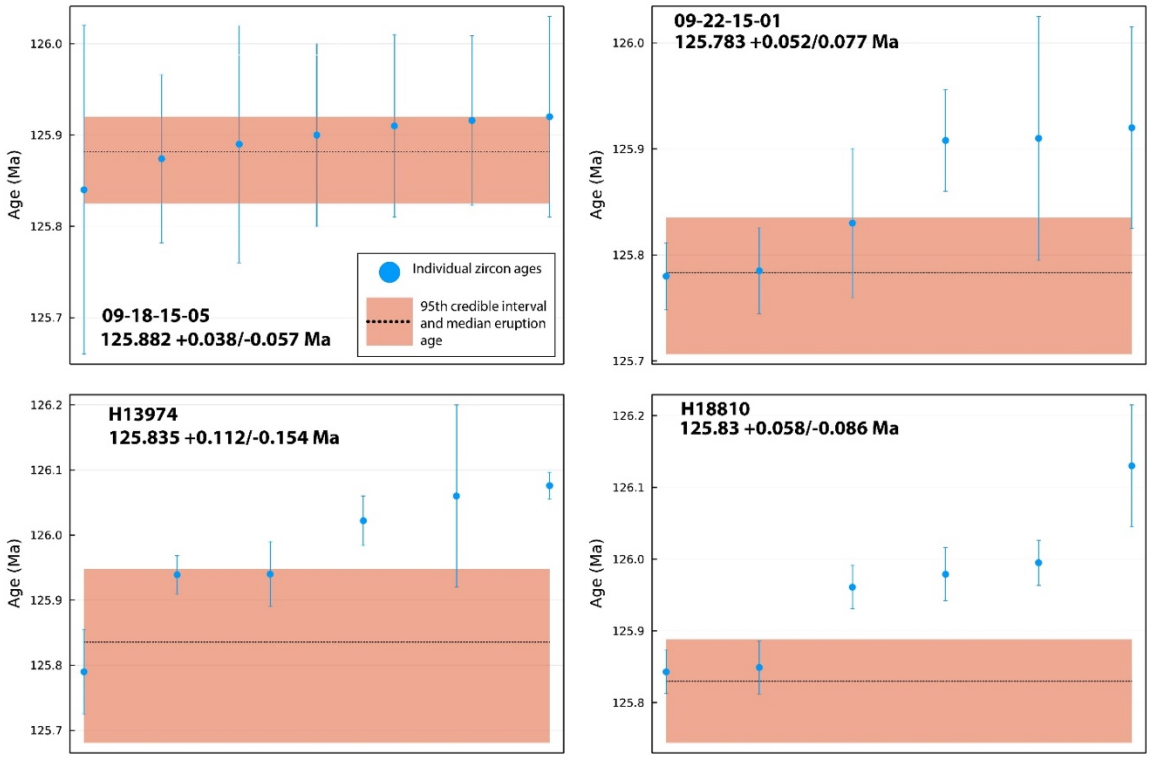


Fig. S18. Rank order plots for the four dated horizons. In these figures, the individual zircon ages with their associated 2σ uncertainties are shown. The stippled lines and orange shaded areas show the median eruption age estimate and 9^{5th} percentile credible interval for the eruption age estimate distribution for each sample. The median age and 95th percentile credible interval were used an inputs for the stratigraphic age-depth model

Fig. S19.

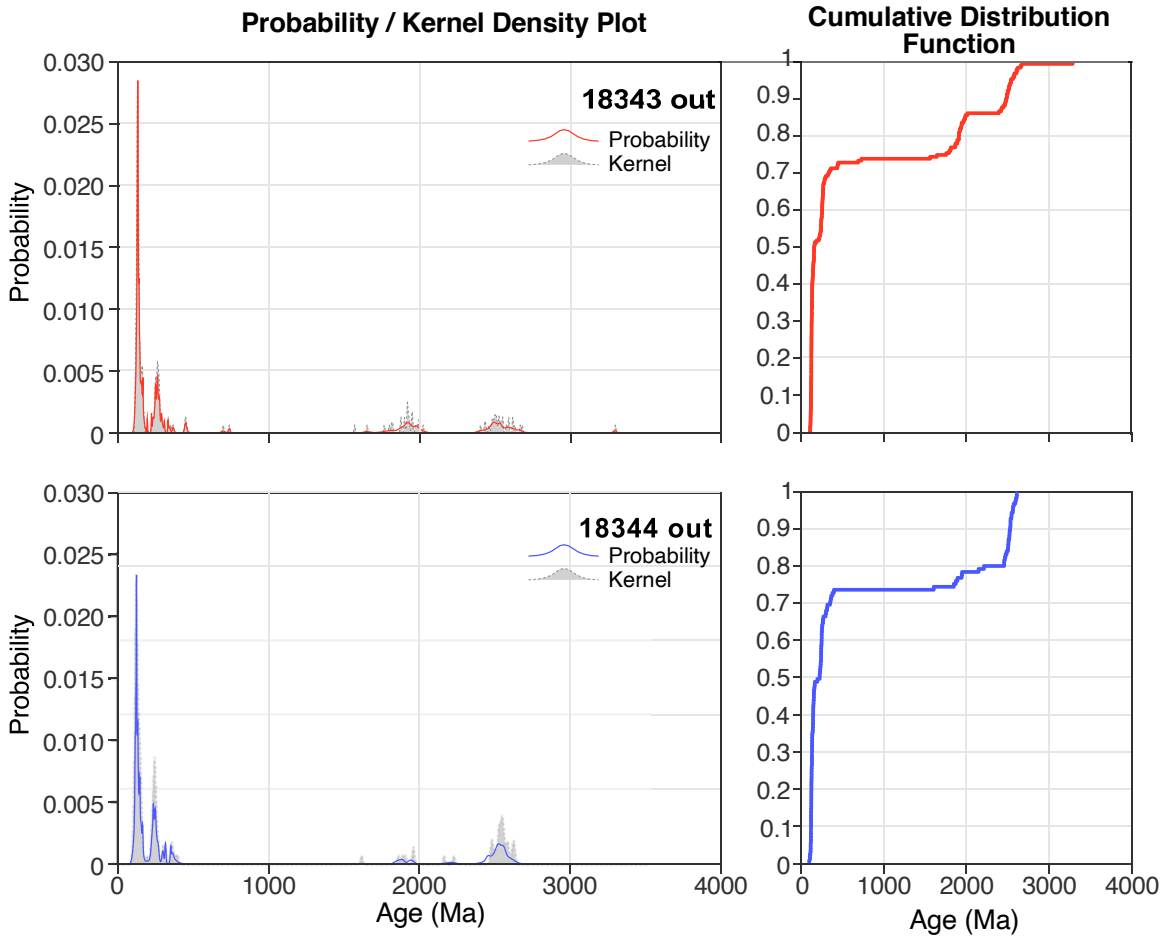


Fig. S19. Probability and kernel density and cumulative distribution plots of detrital zircons from matrix of the *Psittacosaurus* dinosaurs.

Fig. S20.

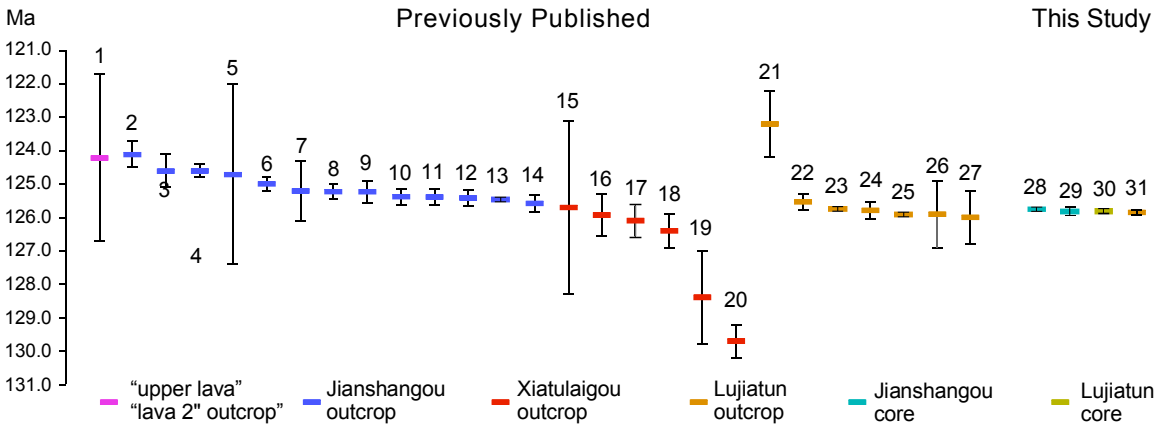


Fig. S20. Previously published data parsed out along a vertical time axis with means (thick horizontal bars) and 2-sigma uncertainties compared to results from this this study. From Table S4.

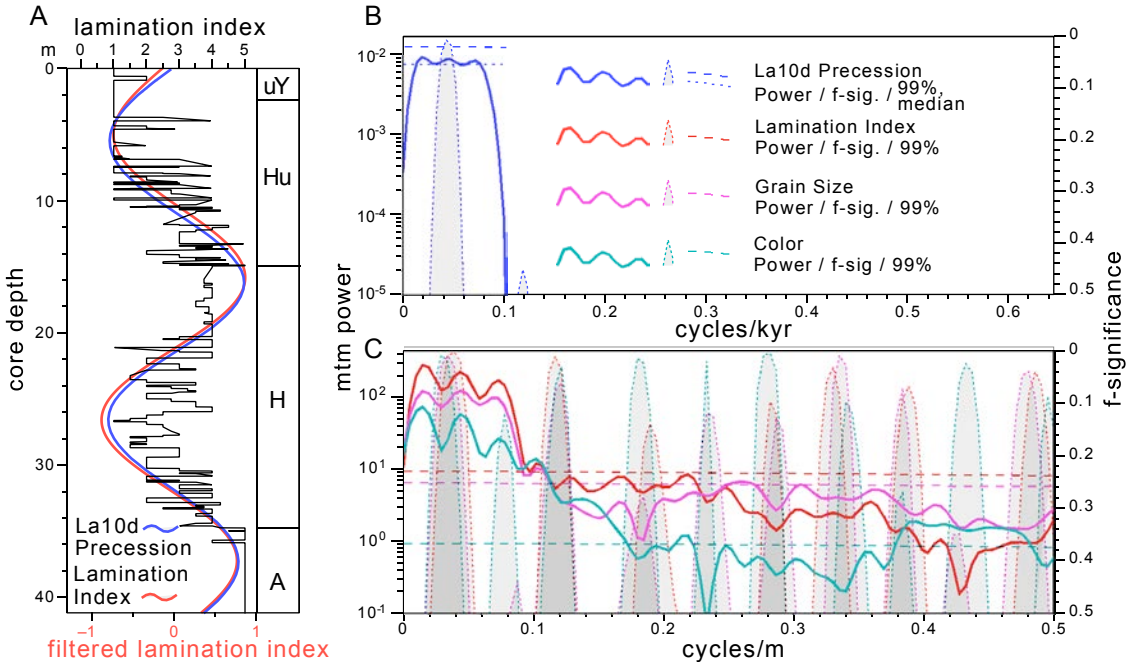


Fig. S21. Time series analysis of the lamination index data (Available in Dataset S1) of the Anjiagou through overlying undivided Yixian Formation in the Huangbanjiagou no. 1 core and adjacent outcrop showing fit with climatic precession assuming an accumulation rate based on our preferred age model employing the three successive dates in the section (samples a, b and c in Figure 2 in the main text)). **A**, Lamination index for core and outcrop with filtered lamination index of Anjiagou through top of section. Red curve represents the fit to the filtered lamination index (0.0486±0.0100 cycles/m). The blue curve is the La10d solution from 125.779 - 125.856 Ma with a period of 21.7 kyr, which was selected to match the shape of the filtered Yixian data. Abbreviations of lithostratigraphic units are: uY, undivided Yixian Formation; Hu, Huangbanjigou Bed, Jianshangou Member; H, Hengdaozi Bed, Jianshangou Member; A, Anjiagou Bed, Jianshangou Member; D, Dajianshanzi Bed, Jianshangou Member; X, position of Xiatulaigou Member, cut out; L, Lujiatun Member. **B**, Power spectrum (2π MTM) of the precession index in A, with a peak period and f-significance at 23.4 kyr (only top section to base Anjiagou Bed), indistinguishable from the peak lithological cycle period (within bandwidth uncertainty). **C**, Power spectrum (2π MTM) of lamination index, color and grains size for the core and outcrop in A with peak power and f-significance at 29.4 m/cycle. Our preferred accumulation rate of 136.7 cm / kyr gives a period of 21.5 kyr to this 29.4 m cycle, and using the TimeOpt accumulation rate of 128.153 cm / kyr (Fig. S22) yields a period of 22.9 kyr which is excellent agreement.

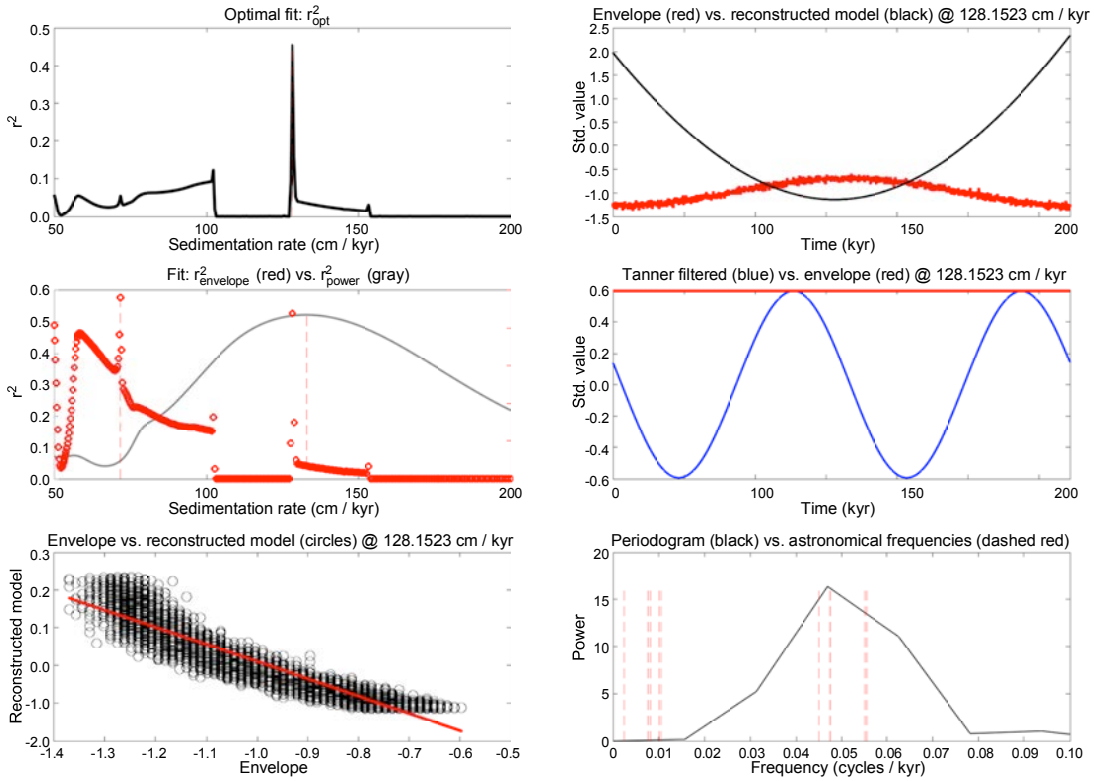


Fig. S22. TimeOpt analysis of the detrended lamination index data (Fig. 2B) using the following parameters. Tested accumulation rate, min 50 cm/kyr, max 200 cm/kyr, number 300. Frequency, middle age of data 126 Ma; Fit to precession modulation; Tanner bandpass cut-off frequencies, low 0.0370, high 0.0687, roll-off 10^12; correlation method was Spearman.

Table S1. Locations of Cores and Outcrops.

Name of core or outcrop	Latitude	Longitude
Huangbanjigou no. 1 core	41.611806°	120.833472°
Sihetun no. 1 core	41.589776°	120.793713°
Jianshangou no. 1 core	41.602000°	120.844167°
Sanbaoyingcun outcrop	41.541430°	120.842413°

Table S2. CA-TIMS data summary.

Sample ID	N	Median eruption age (Ma)	95th Credible Interval (Myrs)	
09.22.15-01	7	125.783	-0.080	+0.053
H1-3794	7	125.835	-0.160	+0.118
H1-8810	9	125.830	-0.090	+0.058
09-18-15-05	7	125.882	-0.055	+0.038

Table S3. LA-ICP-MS Summary

Sample	Youngest zircon (Ma)	Youngest 2+ grains at 1σ	Youngest 3+ grains at 2σ	Youngest peak (Ma)
18343	113.8 +/- 5.2	119.8 +/- 2.06 (MSWD = 0.32, n =20)	124.57 +/- 0.91 (MSWD = 1.29, n = 45)	128 (n = 64)
18344	97.4 +/- 8.6	104.23 +/- 8.52 (MSWD = 0.43, n = 3)	116.5 +/- 1.99 (MSWD = 0.99, n = 6)	124 (n = 40)
18344*	106.0 +/- 6.0	112.42 +/- 6.1 (MSWD = 0.61, n = 22)	118.89 +/- 1.32 (MSWD = 1.13, n = 26)	124 (n = 40)

*youngest grain removed

Table S4. Sources of published dates in Main Text Fig. 2

Number Fig. 2	Unit	Age (Ma)	s	Method	Reference
1	"upper lava"	124.2	2.5	Ar-Ar, groundmass	Zhu et al., 2007
2	Jianshangou	125.457	0.051	IRMS U/Pb zircon	Zhong et al., 2021(27)
3	Jianshangou	125.22	0.22	Ar-Ar, groundmass	Chang et al., 2017(28)
4	Jianshangou	125.2	0.9	Ar-Ar, whole rock	Wang et al., 2001(29)
5	Jianshangou	125.0	0.2	Ar-Ar, sanidine	Swisher et al., 2002(30)
6	Jianshangou	124.7	2.7	SHRIMP U/PB, zircon	Yang et al., 2007(31)
7	Jianshangou	124.6	0.5	Ar-Ar, sanidine	Swisher et al., 1999(32)
8	Jianshangou	124.6	0.2	Ar-Ar, sanidine	Swisher et al., 1999(32)
9	Jianshangou	124.1	0.4	Ar-Ar, sanidine	Chang et al., 2009(33)
10	Jianshangou	125.23	0.33	Ar-Ar, sanidine	Li et al., 2022(23)
11	Jianshangou	125.37	0.24	Ar-Ar, sanidine	Li et al., 2022(23)
12	Jianshangou	125.38	0.24	Ar-Ar, sanidine	Li et al., 2022(23)
13	Jianshangou	125.41	0.24	Ar-Ar, sanidine	Li et al., 2022(23)
14	Jianshangou	125.57	0.25	Ar-Ar, sanidine	Li et al., 2022(23)
15	Xiatulaigou	129.7	0.5	Ar-Ar, groundmass	Chang et al., 2009(33)
16	Xiatulaigou	128.4	1.4	Ar-Ar, whole rock	Wang et al., 2001(29)
17	Xiatulaigou	126.4	0.5	Ar-Ar, groundmass	Chang et al., 2009(33)
18	Xiatulaigou	126.1	0.5	Ar-Ar, groundmass	Chang et al., 2009(33)
19	Xiatulaigou	125.920	0.620	Ar-Ar, groundmass	Chang et al., 2017(28)
20	Xiatulaigou	125.7	2.6	Ar-Ar, whole rock	Zhu et al., 2007(34)
21	Lujiatun	126.0	0.8	Ar-Ar, bulk K-feldspar?	Chang et al., 2019(35)
22	Lujiatun	125.9	1.0	Ar-Ar, bulk K-feldspar?	Chang et al., 2019(35)
23	Lujiatun	125.884	0.060	IRMS U/PB, zircon	Zhong et al., 2021(27)
24	Lujiatun	125.755	0.061	IRMS U/PB, zircon	Zhong et al., 2021(27)
25	Lujiatun	123.2	1.0	Ar-Ar, bulk K-feldspar?	He et al., 2006(36)
26	Lujiatun	125.54	0.25	Ar-Ar, sanidine	Li et al., 2022(23)
27	Lujiatun	125.79	0.26	Ar-Ar, sanidine	Li et al., 2022(23)
28	Jianshangou	125.783	0.053	TIMS U/PB, zircon	this study 09.22.15-01
29	Jianshangou	125.829	0.118	TIMS U/PB, zircon	this study H1-3794
30	Lujiatun	125.828	0.058	TIMS U/PB, zircon	this study H1-8810
31	Lujiatun	125.882	0.038	TIMS U/PB, zircon	this study 09.18.15-05

Dataset S1 (separate file). Dataset_SI_1_TIMS_U-Pb_zircon_data_table.xls are the zircon CA-ID-TIMS data.

Dataset S2 (separate file). Dataset_SI_2_IVPP_18343_data table.xls are the zircon LA-ICP-MS data for IVPP 18343.

Dataset S3 (separate file). Dataset_SI_2_IVPP_18344_data table.xls are the zircon LA-ICP-MS data for IVPP 18344.

Dataset S4 (separate file). Dataset_SI_4_haungbanjigou1_jianshangou_stratigraphic_data.xlsx are the stratigraphic depth, qualitative color, depth rank, and grain size used in time series analysis.

Dataset S5 (separate file). Dataset_SI_5_granulometry_data.xlsx are the lasersizer data for the two dinosaur specimens.

SI References

1. Y. Pan, C. Guan, E. Gong, Stratigraphy, Fossils, and Palaeoenvironments of the Middle Jurassic and Early Cretaceous Rocks of Western Liaoning and adjacent Inner Mongolia - Field Guide. *Field Guide, The 2nd Symposium of international Geoscience Programme Project 632, September 14-19, 2015*, 1-29 (2015).
2. J. M. Mattinson, Zircon U–Pb chemical abrasion ("CA-TIMS") method: combined annealing and multi-step partial dissolution analysis for improved precision and accuracy of zircon ages. *Chemical Geology* **220** (2005).
3. D. J. Condon, B. Schoene, N. M. McLean, S. A. Bowring, R. R. Parrish, Metrology and traceability of U–Pb isotope dilution geochronology (EARTHTIME Tracer Calibration Part I). *Geochimica et Cosmochimica Acta* **164**, 464-480 (2015).
4. N. M. McLean, D. J. Condon, B. Schoene, S. A. Bowring, Evaluating uncertainties in the calibration of isotopic reference materials and multi-element isotopic tracers (EARTHTIME Tracer Calibration Part II). *Geochimica et Cosmochimica Acta* **164**, 481-501 (2015).
5. T. Krogh, A low-contamination method for hydrothermal decomposition of zircon and extraction of U and Pb for isotopic age determinations. *Geochimica et Cosmochimica Acta* **37**, 485-494 (1973).
6. A. O. Nier, A redetermination of the relative abundances of the isotopes of carbon, nitrogen, oxygen, argon, and potassium. *Physical Review* **77**, 789 (1950).
7. J. Hiess, D. J. Condon, N. McLean, S. R. Noble, 238U/235U systematics in terrestrial uranium-bearing minerals. *Science* **335**, 1610-1614 (2012).
8. U. Schärer, The effect of initial230Th disequilibrium on young UPb ages: the Makalu case, Himalaya. *Earth and Planetary Science Letters* **67**, 191-204 (1984).
9. L. L. Claiborne *et al.*, Zircon as magma monitor: Robust, temperature-dependent partition coefficients from glass and zircon surface and rim measurements from natural systems. *Microstructural geochronology: Planetary records down to atom scale*, 1-33 (2018).
10. C. B. Keller, B. Schoene, M. Barboni, K. M. Samperton, J. M. Husson, Volcanic–plutonic parity and the differentiation of the continental crust. *Nature* **523**, 301-307 (2015).
11. J. F. Bowring, N. M. McLean, S. Bowring, Engineering cyber infrastructure for U-Pb geochronology: Tripoli and U-Pb_Redux. *Geochemistry, Geophysics, Geosystems* **12** (2011).
12. N. M. McLean, J. F. Bowring, S. A. Bowring, An algorithm for U-Pb isotope dilution data reduction and uncertainty propagation. *Geochemistry, Geophysics, Geosystems* **12** (2011).

13. A. Jaffey, K. Flynn, L. Glendenin, W. t. Bentley, A. Essling, Precision measurement of half-lives and specific activities of U 235 and U 238. *Physical review C* **4**, 1889 (1971).
14. C. B. Keller, B. Schoene, K. M. Samperton, A stochastic sampling approach to zircon eruption age interpretation. *Geochemical Perspectives Letters* **8**, LLNL-JRNL-738859 (2018).
15. B. Schoene *et al.*, U-Pb constraints on pulsed eruption of the Deccan Traps across the end-Cretaceous mass extinction. *Science* **363**, 862-866 (2019).
16. G. E. Gehrels, V. A. Valencia, J. Ruiz, Enhanced precision, accuracy, efficiency, and spatial resolution of U-Pb ages by laser ablation–multicollector–inductively coupled plasma–mass spectrometry. *Geochemistry, Geophysics, Geosystems* **9** (2008).
17. G. Gehrels, V. Valencia, A. Pullen, Detrital zircon geochronology by laser-ablation multicollector ICPMS at the Arizona LaserChron Center. *The Paleontological Society Papers* **12**, 67-76 (2006).
18. J. t. Stacey, J. Kramers, Approximation of terrestrial lead isotope evolution by a two-stage model. *Earth and planetary science letters* **26**, 207-221 (1975).
19. Y. Wang *et al.*, Stratigraphy, correlation, depositional environments, and cyclicity of the Early Cretaceous Yixian and ?Jurassic-Cretaceous Tuchengzi formations in the Sihetun area (NE China) based on three continuous cores. *Palaeogeography, Palaeoclimatology, Palaeoecology* **464**, 110-133 (2016).
20. H. Wu *et al.*, Astrochronology for the Early Cretaceous Jehol Biota in northeastern China. *Palaeogeography, Palaeoclimatology, Palaeoecology* **385**, 221-228 (2013).
21. S. R. Meyers, The evaluation of eccentricity-related amplitude modulation and bundling in paleoclimate data: An inverse approach for astrochronologic testing and time scale optimization. *Paleoceanography* **30**, 1625–1640 (2015).
22. M. Li, L. Hinnov, L. Kump, Acycle: Time-series analysis software for paleoclimate research and education. *Computers & Geosciences* **127**, 12–22 (2019).
23. Y. Li *et al.*, Rapid preservation of Jehol Biota in Northeast China from high precision 40Ar/39Ar geochronology. *Earth and Planetary Science Letters* **594**, 117718 (2022).
24. R. Y. Anderson, Enhanced climate variability in the tropics: a 200 000 yr annual record of monsoon variability from Pangea's equator. *Climate of the Past* **7**, 757-770 (2011).
25. D. V. Kent, G. Muttoni, P. Brack, Magnetostratigraphic confirmation of a much faster tempo for sea-level change for the Middle Triassic Latemar platform carbonates. *Earth and Planetary Science Letters* **228**, 369-377 (2004).
26. G. Bond *et al.*, A pervasive millennial-scale cycle in North Atlantic Holocene and glacial climates. *Science* **278**, 1257-1266 (1997).
27. Y. Zhong *et al.*, High-Precision geochronological constraints on the duration of 'Dinosaurs Pompeii' and the Yixian Formation. *National Science Review* **8**, nwab063 (2021).
28. S. Chang, K. Q. Gao, C. F. Zhou, F. Jourdan, New chronostratigraphic constraints on the Yixian Formation with implications for the Jehol Biota. *Palaeogeography, Palaeoclimatology, Palaeoecology* **487**, 399-406 (2017).
29. S. Wang, G. Hu, P. Li, Y. Wang, Further discussion on the geologic age of Sihetun vertebrate assemblage in western Liaoning, China: evidence from Ar/Ar dating. *Acta Petrologica Sinica* **17**, 663–668 (2001).
30. C. C. Swisher *et al.*, Further support for a Cretaceous age for the feathered-dinosaur beds of Liaoning, China: New 40Ar/39Ar dating of the Yixian and Tuchengzi formations. *Chinese Science Bulletin* **47**, 136–139 (2002).
31. W. Yang, S. Li, B. Jiang, New evidence for Cretaceous age of the feathered dinosaurs of Liaoning: zircon U-Pb SHRIMP dating of the Yixian Formation in Sihetun, northeast China. *Cretaceous Research* **28**, 177–182 (2007).
32. C. C. Swisher, Y. Q. Wang, X. L. Wang, X. Xu, Y. Wang, Cretaceous age for the feathered dinosaurs of Liaoning, China. *Nature* **400**, 58–61 (1999).
33. S. Chang, H. Zhang, P. R. Renne, Y. Fang, High-precision 40Ar/39Ar age for the Jehol Biota. Palaeogeogr. Palaeoclimatol. Palaeoecol. . *Palaeogeography, Palaeoclimatology, Palaeoecology* **280**, 94–104 (2009).
34. R. X. Zhu, Y. X. Pan, R. P. Shi, Q. S. Liu, D. M. Li, Palaeomagnetic and 40Ar/39Ar dating constraints on the age of the Jehol Biota and the duration of deposition of the Sihetun

fossil-bearing lake sediments, northeast China. *Cretaceous Research* **28**, 171–176 (2007).
35. S. Chang, New age constraints on the Yixian Formation and its implications for the Jehol Biota. *PaleoBios* **36**, 97 (2019).
36. H. Y. He *et al.*, 40Ar/39Ar dating of Lujiatun bed (Jehol Group) in Liaoning, northeastern China. *Geophysical Research Letters* **33**, L04303 (2006).